

Accounts

Exterior Characteristics of Molecular Orbitals and Molecular Surfaces as Studied by Atomic Probes

Koichi Ohno

Department of Chemistry, Graduate School of Science, Tohoku University, Aramaki, Aoba-ku, Sendai 980-8578

Received October 1, 2003; E-mail: ohnok@qpcrkk.chem.tohoku.ac.jp

This is a brief survey of studies on exterior characteristics of molecules conducted by means of atomic probes, mostly by metastable states of rare gas atoms in collisional ionization experiments and partly by atoms from H to Ar in quantum chemical calculations. Spatial distributions of molecular orbitals (MO) outside the molecular surfaces have been studied to determine stereoelectronic properties related with partial ionization cross sections of molecules due to electrophilic attacks of metastable atoms. A newly developed collision-energy/electron-energy resolved two-dimensional electron spectroscopy has disclosed anisotropic and dynamic characteristics of molecular surfaces (MS) via collision-energy dependence of partial ionization cross sections. Starting from a simple theoretical model of exterior electron densities (EED), researchers have developed quantum chemical treatments of the ionization reactions to a level of trajectory calculations based on potential energy surfaces of both entrance and exit reaction channels together with electronic transition rates between the surfaces. The present stage of techniques can elucidate one of the two aspects, MO or MS, assuming knowledge of the other. Since experimental aspects may contain various features of MO and MS, a simultaneous determination of both MO and MS by experiments will allow further developments in experimental techniques.

Exterior parts of molecules are of great importance in chemical phenomena and physical properties, because it is through them that molecules usually interact with each other. Exterior characteristics of molecules are related to their molecular orbitals and molecular surfaces. Molecular orbitals play dominant roles in electron transfer or electron exchange in connection with reduction–oxidation (redox) processes, excitation energy transfer, and production or dissociation of chemical bonds. Molecular surfaces govern various properties, such as molecular shape and intermolecular forces, due to repulsive and attractive interactions. A molecule's shape excludes other three-dimensional bodies from the interior parts of its own body, and hence it determines the reactant accessible areas. Intermolecular forces lead to adsorption, association, and formation of molecular complexes and clusters as well as formation of condensed phases.

Although molecular orbitals were introduced on purely theoretical grounds, experimental observation of the orbital pattern was suggested by Fukui[1] on the basis of successful studies on chemical reactions by molecular orbital theories.[2,3] Various electron spectroscopic techniques have been employed to study molecular orbitals experimentally. Ionization energies observed by photoelectron spectroscopy[4–6] have been compared with theoretical orbital energies in many cases where Koopmans' theorem[7] is valid. Experimental momentum distributions for individual orbitals obtained by (e, 2e) electron spectroscopy have been used to test the quality of theoretically obtained molecular orbital functions.[8–15] Although photons and electrons are excellent probes to obtain information about molecular properties in general, local characteristics of molecules, especially in the chemically important exterior regions, are more sensitively studied by atomic probes. Atoms interact with molecules strongly on their molecular surfaces, whereas most photons and electrons penetrate through the molecules because of their relatively very low cross sections.

The external surface of a molecule is of great significance when it meets with other chemical species. An outer boundary surface of a molecule that divides the exterior regions from the interior region can be defined as the molecular surface. The concept of molecular surfaces is also important for recognition of shapes of molecules.[16] The most primitive description of molecular surfaces and molecular bodies can be constructed as the van der Waals contour, a union of the constituent atomic spheres.[17] Such surfaces are known as the van der Waals surfaces. Along with similar surfaces known as the solvent contact surfaces and the solvent exclusion surfaces,[18] they have been used in many fields, such as biosciences[19] and analytical chemistry.[20] Although these surfaces are useful, some inaccuracies may be expected when one uses van der Waals radii regardless of local circumstances. van der Waals radii should depend on the kind of atoms interacting with each other. Anisotropy of the van der Waals radii should be considered when the molecular system is highly anisotropic. The van der Waals surface as the boundary to the incoming species should vary with the rel-

Published on the web May 6, 2004; DOI 10.1246/bcsj.77.887

ative velocities of collisions in scattering experiments and also with the forces exerted in atomic force experiments.

This account presents an overview of our investigations for two decades in attempting to look into exterior characteristics of molecular orbitals and molecular surfaces by means of atomic probes. Our motivation has been cultivated by the strong relationships between the molecular orbital theory and the organic reaction chemistry.[2,3] Since organic reactions are explained by spatial characteristics of molecular orbitals, electron distributions of molecular orbitals should also be elucidated by some experiments along the converse direction, provided that the phenomena can be directly connected with molecular orbital functions. It was a Penning ionization experiment[21] that triggered the author to engage in the present investigations which include a number of long troublesome challenges to develop new experimental techniques and theoretical treatments.

1. Study of Stereoelectronic Properties of Molecular Orbitals by Penning Ionization Electron Spectroscopy

When a molecule (M) collides with an excited atom (A^*) with an energy higher than the ionization energy (IE) of M, an electron transfer process can occur to yield an ionic state of M (M^+) and the ground state of the atom A together with an ejected electron (e^-);

$$A^* + M \rightarrow A + M^+ + e^-. \quad (1)$$

This process is known as Penning ionization,[22] where A^* is a metastable rare gas atom, such as $He^*(2^3S)$, $He^*(2^1S)$, $Ne^*(^3P_{0,2})$, and $Ar^*(^3P_{0,2})$, whose excitation energies[23,24] are comparable with UV resonance photon energies of a rare gas discharge, as shown in Table 1. Analysis of the kinetic energies (E_e) of ejected electrons gives a Penning ionization electron spectrum (PIES),[25] which is similar in many respects to a UV photoelectron spectrum (UPS).[5,6] Electron energies E_e can be related to ionization energies IE, which are the absolute values of self-consistent molecular orbital energies in Koopmans' theorem:[7] $E_e = E - IE - \delta$, where E is the energy of the excited atom or the photon and δ is the energy balance due to the relative motion of the particles. Although for UPS δ is always negligible, for PIES δ depends on the distance between M and A^* at the instance of the electron ejection.[26] This quantity δ for PIES is usually much less than a few hundred meV. Therefore, UPS and PIES show very similar ionization spectra in the electron energy scales. Since observed bands in UPS for most closed shell molecules have been assigned to occupied molecular orbitals,[4–6] most of the spectral bands in PIES can also be ascribed to individual molecular orbitals. Thus, these electron spectroscopic techniques can provide some information on molecular orbitals.

Table 1. Excitation Energies and Resonance Photon Energies of Rare Gas Atoms

Excitation	Energy/eV	Resonance	Photon energy/eV
$He^*(2^3S)$	19.820	He I	21.217
$He^*(2^1S)$	20.616		
$Ne^*(^3P_2)$	16.619	Ne I	16.671
$Ne^*(^3P_0)$	16.715		16.848
$Ar^*(^3P_2)$	11.548	Ar I	11.623
$Ar^*(^3P_0)$	11.723		11.823

It is well known that the relative band intensities in UPS are nearly the same when the comparison is made among ionization bands originating from molecular orbitals that are composed of the same set of atomic orbitals.[27] Therefore, it is difficult to obtain direct experimental information on spatial electron distributions of molecular orbitals from photoelectron spectra. On the other hand for PIES, ionization cross sections or ionization reaction probabilities can be related with the spatial characteristics of molecular orbitals, because Penning ionization has been considered as an electron-exchange type process.[28]

As shown in Fig. 1(a), a metastable $He^*(2^3S)$ atom as A^* reacts as an electrophile to attack an occupied molecular orbital ϕ_i of the target molecule M, from which an electron is transferred into the vacant inner-shell orbital χ_{1s} of He^*, and an electron is ejected from the occupied outer-shell orbitals χ_{2s} of He^* into a continuum-state orbital φ_e to be detected as an ejected electron. A simple principle for orbital activities in Penning ionization reactions can be established on the basis of the electron-exchange model, where the mutual overlap of involved orbitals plays key roles in electron transfer processes. It should also be noted that the metastable atom A^* cannot penetrate into the molecular surface of M, which is the repulsive boundary against the incoming A^*. As shown in Fig. 1(b), $He^*(2^3S)$ atoms as A^* can approach the molecule M up to the molecular surface. Electron transfer from M to $He^*(A^*)$ can easily take

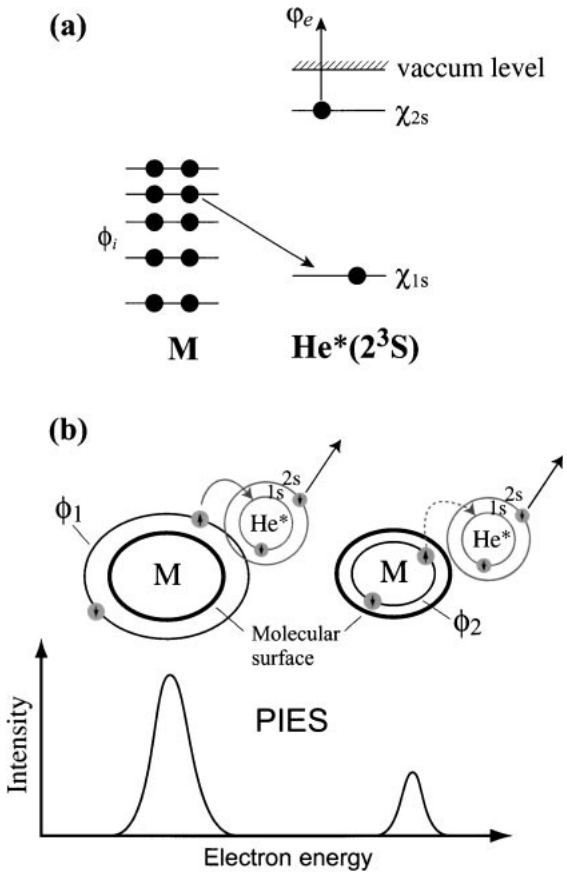

Fig. 1. (a) Process of Penning ionization. (b) The principle for the relationship between the spatial electron distribution of the molecular orbital and the relative PIES intensity.

place for the outer orbital ϕ_1 which has a large overlap with the vacant inner-shell orbital of He*(A*) rather than for the inner orbital ϕ_2 which does not extend much into the exterior region. Thus, the outer orbital exposed to the outside gives a higher intensity in PIES than does the inner orbital localized in the inside. This stereoelectronic principle was evidenced by the first systematic inspection of relative band intensities in PIES of various inorganic and organic compounds, on the basis of careful corrections of the transmission efficiency of the electron spectrometer,[29] though the earlier studies had compared intensity distributions between PIES and UPS.[30–33] The introduction of the molecular surface as the repulsive boundary surface,[29] which separates the exterior reactive regions from the interior inactive parts in Penning ionization, removed many difficulties found in earlier studies.

In the case of N_2, CO, and CN compounds, σ orbitals corresponding to lone-pair orbitals were found to give remarkably enhanced PIES bands with respect to π bands.[30–32] A reverse tendency was found in PIES of unsaturated hydrocarbon molecules for which π bands were found to be much more enhanced than the σ bands.[33] This formal contradiction was removed by the principle of Penning ionization; PIES intensities are not governed by the orbital symmetry but by the extent of the exterior electron distributions. Further studies of PIES intensities[34–44] revealed relative activities of various kinds of molecular orbitals as listed in Table 2. For linear inorganic molecules, σ orbitals with some nonbonding characters give much larger activities in Penning ionization than π orbitals, while for unsaturated hydrocarbons π orbitals give much higher activities than σ orbitals as mentioned above. In the case of unsaturated hydrocarbons, some interesting differences were found among σ orbitals; σ(CH) type orbitals are more active than σ(CC) type orbitals, because CC bonding orbitals are much more localized on the bonding region where metastable rare gas atoms cannot attack.[29,36] Relative activities of nonbonding orbitals (n) were found to be large with respect to those of bonding orbitals (b) for both inorganic[29] and organic[39] molecules. Very high activities of nonbonding orbitals were compared for various types of lone-pair orbitals. The outer valence shell[39,40] and the lower electron negativities in the order of groups 15(V) > 16(VI) > 17(VII) in the periodic table[39,41] were found to yield higher activities, because of the larger extent of electron distributions in the exterior regions. The tendency of σ(n) > π was also found for organic systems with a CN or CO group having an N or O atom, which is more electronegative than a C atom.[35,42] Spatially localized orbitals inside the molecules were found to be much less active.[43,44] Typical examples are metal complexes and organometallic compounds with a central metal atom and some ligands surrounding the metal atom. These propensities are well understood by the above-mentioned stereoelectronic principle of Penning ionization, which is governed by spatial distributions of molecular orbitals and strong limitations of accessible regions for incoming reactant atoms. The connection of the reactivity with the shape of the relevant orbitals was pointed out by Hoffmann,[45] and this connection is called the isolobal analogy by Mingos.[46] The above findings in Penning ionization also demonstrate the isolobal effects on collisional ionization processes.[35,47]

Stereoelectronic properties of molecular orbitals were disclosed for many molecules by a series of systematic studies.[41,47–50] Effects of through-space and through-bond interactions[51] on electron distributions of molecular orbitals were studied for 1,4-diazabicyclo[2.2.2]octaene (DABCO) and norbornadiene.[48] Figure 2 shows an example of the through-bond interaction by which the antisymmetric type nonbonding orbital (n_a) of DABCO is more active with the larger exterior electron distribution than the symmetric type nonbonding orbital (n_s). The through-bond interaction in the n_s orbital causes strong absorption of electron densities into bonding regions and hence a decrease of exterior electron densities, to result in a considerable reduction of the efficiency in the electrophilic reaction of the n_s orbital. An example of the through-space interaction was observed for norbornadiene: the symmetric type π orbital (π_s) was found to be more active than the antisymmetric type π orbital (π_a). This indicates that the exterior electron distributions in the endo face are effectively increased for the π_s orbital by through-space interaction that switches on the extraction of electron densities outside the molecular surface into the exterior region to enhance the efficiency of the electrophilic reaction of the π_s orbital.

Steric effects were observed for the geometrical accessibility of metastable atoms. Figure 3 shows relative PIES and UPS activities of π and n orbitals in substituted anilines with methyl groups.[49] The ratios for UPS are almost constant indicating that photoionization cross sections are nearly equal for molecular orbitals composed of similar type atomic orbitals.[27] Therefore UPS does not show substitution effects in the relative intensities. On the other hand, relative PIES intensities exhibit remarkable substitution effects. Depending on the number of methyl substitution on the ring, I(n)/I(π_2) increases, whereas this ratio decreases when the substitution is introduced on the amino group. Since methyl groups are bulky obstacles for metastable

Table 2. Relative Activity of Molecular Orbitals in Penning Ionization

Tendency	Example	Reference
σ(n) > π	N_2, CO, CO_2, N_2O	29, 30, 34, 35
$\pi > \sigma_{CH} > \sigma_{CC}$	C_2H_2, C_2H_4, C_6H_6	29, 33, 36
	$C_{10}H_8$, $C_{14}H_{10}$	37, 38
n > b	NH_3, H_2O, H_2S	29
	RX (X = NH_2, SH, Cl, Br, I)	39
n_X: 5p > 4p > 3p > 2p	RX (X = Cl, Br, I, F)	39, 40
n_X: V > VI > VII	RX (X = NH_2, OH, F, SH, Cl)	39, 41
nsp > π	RCN, RCOR′	35, 42
Ligand > Metal-d	$Fe(C_5H_5)_2$, $Fe(CO)_5$	43, 44

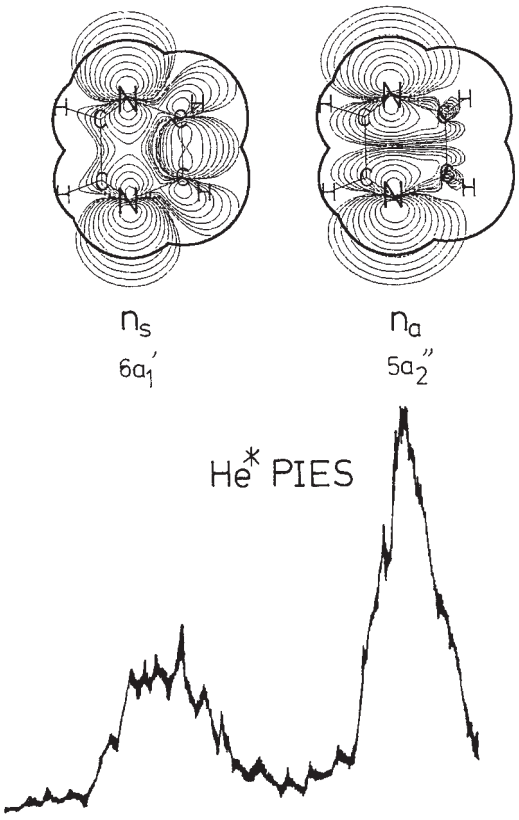

Fig. 2. He*(2^3S) PIES and electron density contour plots of the symmetric nonbonding orbital (n_s) and the antisymmetric nonbonding orbital (n_a) for 1,4-diazabicyclo[2.2.2]-octane (DABCO).[48] HOMO is n_s with IE = 7.60 eV, and the next HOMO is n_a with IE = 9.64 eV. Thick solid curves in the map indicate the repulsive molecular surface.

atoms to approach the target orbitals, the methyl substitution causes strong steric effects decreasing the PIES activities of nearby orbitals.

Subtle changes of electron populations depending on chemical structures were probed by metastable atoms.[50] A systematic study of PIES activities in $(CH_3)_4M$ (M = C, Si, Ge, Sn, Pb) showed that the relative activity of σ(MC) orbitals with respect to σ(CH) orbitals decreases with the sizes of the central atom M. This is because, on going from C to Pb, the interactions between M and the methyl group become weaker, associated with the considerable decrease of the IE value for the M atom.

Dynamic effects on exterior electron distributions were observed for hydrogen bonding systems.[41] When a hydrogen bond is formed in a molecule such as XCH_2CH_2OH, the PIES activity of the nonbonding orbital related to the lone-pair electrons contributing to the hydrogen bond decreases. An analysis of the temperature dependence showed that dissociation of the hydrogen bond causes the recovery of the activity of the nonbonding orbital, because the steric shield against the incoming metastable atoms is taken away at high temperatures.

In order to compare observed relative PIES band intensities with molecular orbital functions, researchers developed the exterior electron density model.[29,36] The exterior electron density (EED) is defined for each molecular orbital ϕ by the following equation:

$$(\mathrm{EED}) = \int_{\Omega} |\phi|^2 \mathrm{d}r. \tag{2}$$

The integration should be taken for the exterior region outside the boundary repulsive molecular surface from which A* cannot penetrate into the inside of the molecule. When the electron density integrated for the interior region is denoted as the interior electron density (IED), then (EED) + (IED) = 1 for each molecular orbital. The repulsive molecular surface is, therefore,

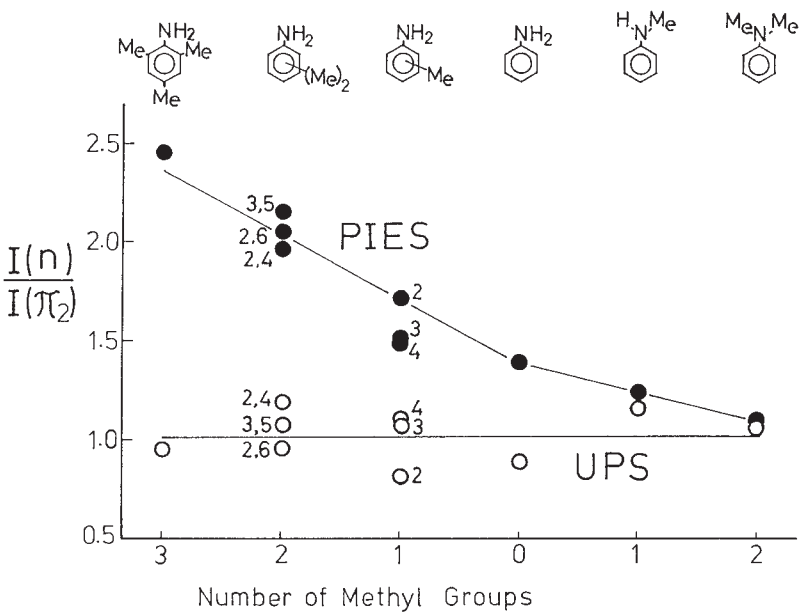

Fig. 3. The integrated intensity ratio for the n and π_2 bands in He*(2^3S) PIES and He I UPS of methyl anilines.[49] Closed circles are for PIES and open circles are for UPS. The studied compounds are shown at the top of the figure. The positions of methylation at the ring are shown beside the circles for mono and dimethylanilines.

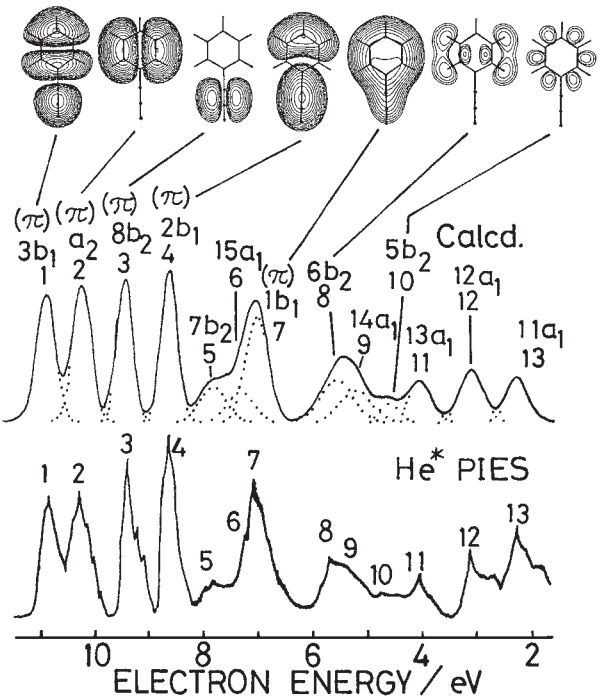

Fig. 4. Observed He*(2^3S) PIES (lower) and calculated EED spectrum (upper) for phenylacetylene and electron density maps.[36] Maps are drawn for some molecular orbitals for a plane 1.7 Å above the molecular plane.

the boundary dividing the inactive part of $|\phi|^2$ (IED) from the reactive part of $|\phi|^2$ (EED). Thus EED has a physical meaning of the relative number of reactive electrons distributed outside the repulsive molecular surface. The EED model gives (1) a relative magnitude for the PIES band intensity and (2) the branching ratio of the ionization reaction, which are considered to be proportional to the partial ionization cross section for the molecular orbital to be ionized. Figure 4 shows a calculated EED spectrum in comparison with the observed He*(2^3S) PIES. Enhanced intensities for π bands in PIES of unsaturated hydrocarbons such as benzene, phenylacetylene, styrene, butadiene, cyclohexene, and cyclohexadiene, were well reproduced by the EED model.[36] The EED model has been successfully applied to many other compounds, naphthalene,[52] anthracene,[38,52] paracyclophane,[53] norbornadiene,[48] DABCO,[48] carbonyl compounds,[35] group 14 (group IV) compounds,[54,55] diphenylchalcogenides,[56] *t*-butylchloride,[55] organic sulfur compounds,[57] and cyclohexanol.[58] It is of note that the orbital activity in Penning ionization is governed by a small amount of EED of ca. 0.01–0.10. In other words, Penning ionization is very sensitive to the EED.

Associated with detailed comparisons of EED calculations with observed PIES activities of molecular orbitals, the following problems have been studied.

(1) Qualities of wave function tails and the basis-set dependence.

(2) Qualities of repulsive molecular surfaces and anisotropic interaction potentials.

(3) Three-dimensional accessibilities of atoms to molecular surfaces in connection with collision trajectories and survival fractions.

EED values were found to depend crucially on the qualities of wave function tails obtained by quantum chemical calculations.[59–62] Small basis sets underestimate EED values especially for nonbonding orbitals. Larger basis sets including diffuse functions yield larger EED values to give better agreement with observed PIES band intensities. Thus, the EED has been used to estimate the qualities of wave function tails theoretically obtained.[59–62] Inclusion of diffuse functions was found to be essential, and reasonable qualities of wave function tails can be checked by comparison with the correct asymptotic decay of Hartree–Fock orbitals.[63–65]

Repulsive molecular surfaces in the EED model for Penning ionization have been estimated as van der Waals (VDW) surfaces composed of spheres with respective VDW radii of the constituent atoms.[29,36,59] VDW surfaces so obtained correspond to widely used space filling models of molecules. The VDW model for repulsive molecular surfaces needed for EED calculations is an approximation of the interaction potential.

The EED concept has been applied to studies of selectivity of organic reactions.[66] In order to consider the anisotropy of reaction probabilities, one can divide the EED into subspaces, two regions divided by a certain plane in a molecule, for example, anti/syn, endo/exo, and axial/equatorial. This variation of the EED model is called the exterior frontier orbital electron (EFOE) density model.[66] Some other applications of the EED model divided into subspaces[50,61] were made prior to the EFOE density model.

Penning ionization spectroscopy studies of solid surface have been made to provide useful information concerning with (1) exterior electron distributions of limited parts of molecular orbitals that are exposed to incoming metastable atoms and (2) orientation and geometrical arrangement of surface molecules. These topics have been reviewed by Harada and co-workers.[67]

2. Development of Collision-Energy/Electron-Energy Resolved Two-Dimensional Penning Ionization Electron Spectroscopy and High-Sensitivity Electron Spectroscopic Techniques

During the studies on stereoelectronic properties of molecular orbitals by Penning ionization electron spectroscopy and the EED model described in the previous section, the concept of molecular surfaces, which divide exterior reactive regions from the interior inactive regions, was used effectively. However, the nature of each molecular surface has not been elucidated. Since Penning ionization processes crucially depend on local characteristics of electron distributions of molecular orbitals, the local nature of molecular surfaces may be probed by metastable atoms. In addition to this, one may vary velocities of metastable atoms to probe the dynamic nature of molecular surfaces, whether they are hard or soft or even adhesive. In the case of attractive potentials related to adhesive interactions, ionization cross sections are expected to decrease with the increase of velocities or collision energies, because the slow He* atoms may be deflected to interact more effectively than the fast He* atoms, as can be seen from Fig. 5. In the case of repulsive potentials, ionization cross sections are expected to increase with the increase of the collision energy, because fast He* atoms may climb up the repulsive wall to approach within a shorter distance, causing a larger overlap between relevant orbitals

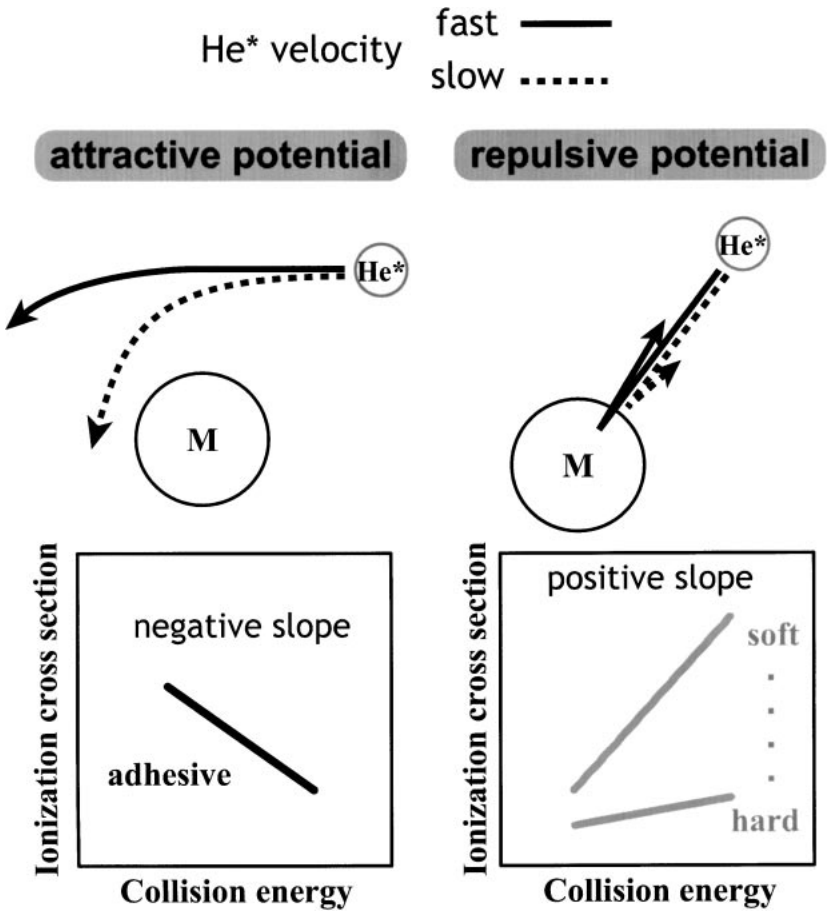

Fig. 5. Adhesive, soft, or hard characteristics of the molecular surface of the molecule M as probed by a He^* atom. A He^* atom with a fast or slow velocity travels along the respective trajectory shown in a solid (fast) or dashed (slow) curve depending on the attractive or repulsive interaction potential. In the collision-energy dependence of ionization cross-sections, adhesive, soft, or hard characteristics can be seen as a negative slope, a steep positive slope, or a much less steep positive slope, respectively.

than slow atoms. Since the penetration of the He^* atoms into the molecular surface becomes more remarkable when the repulsive molecular surface is soft, the increase of the cross section against the increase of the collision energy is expected to be much steeper than that for the hard molecular surface. Thus, the inclination of ionization as a function of the collision energy or the velocity of the colliding particles will give us information on the most important nature of the molecular surface. Based on this scope, the present study has advanced into the next stage concerning the development of collision-energy/electron-energy resolved two-dimensional Penning ionization electron spectroscopy.

There are two important variables in Penning ionization expressed in Eq. 1: one is the kinetic energy of the ejected electron E_e, and the other is the collision energy E_c between two particles A^* and M. When one measures produced ion intensities, then one obtains total ionization cross sections. Total Penning ionization cross sections as functions of E_c have been measured extensively.[68–75] However in many cases several ionic states can be produced. It follows that detection of produced ions does not give any information on individual ionic states, which has been a great obstacle in velocity dependent studies of Penning ionization. Thus it has been a long standing problem to separate total ionization cross sections into partial cross sections for individual ionic states. Another kind of experiment is electron kinetic energy analyses, which provide PIES mentioned in the previous section. Band intensities observed in PIES give branching ratios for various ionic states, which can be related with partial ionization cross sections. In the measurements of PIES, collision energies of A^* have a wide range of thermal energies, and therefore the collision energy dependence has been disregarded, except for the use of two metastable beam sources with different velocity distributions.[34] In these two types of experiments, (1) velocity (or collision energy) selection of A^* and (2) electron kinetic energy analysis have been made separately. Either one of these techniques undergoes considerable reduction of signal intensities due to the selection of a given value of the variables.

Under such circumstances, our efforts have been focused on the development of collision energy-resolved Penning ionization electron spectroscopy.[55,76–83] Velocity selection with a conventional velocity selector passing atoms of a particular velocity reduces the number of A^* atoms by a factor of 10^{-5} (ca. 10^{-3} for the use of a mechanical chopper together with ca. 10^{-2} for a cut of the velocity distribution). When we started this project in 1985, a typical time for one PIES measurement without velocity selection was ca. 3 hrs. This indicates that a velocity resolved PIES measurement requires (10^5 times 3 hrs) = (34

years) and to be continued from 1985 to 2019, unless technical improvements are made. Thus, this condition forced us to improve various parts of our PIES apparatus. At that time we used an electron impact source for production of A* atoms. This kind of metastable source only gave at best the beam intensity of 10^{12} atoms s^{-1} sr^{-1}, even if we used a tandem source with many filaments for electron impacts. We also attempted to use various types of discharge sources employed by many groups, but we could only obtain an intensity of 10^{12} atoms s^{-1} sr^{-1}. After many efforts we read the report of a nozzle discharge source with an intensity of 3×10^{14} atoms s^{-1} sr^{-1}.[84] So we tried this type in 1988. After many improvements and adjustments, we obtained a much higher intensity of 1.6×10^{15} atoms s^{-1} sr^{-1} than previously reported.[77] The advantage of our nozzle discharge source is the collision free part of discharge outside the nozzle, which avoids large amount of de-excitation of A* due to collisions, although considerable reduction of A* intensities by collisions has been inevitable in other beam sources. The development of this very strong source for A* atoms increased our PIES instrument strength by 10^3 times. Figure 6 schematically shows the instrumental development of collision-energy/electron-energy resolved two-dimensional Penning ionization electron spectroscopy. The nozzle discharge source (1) is shown at the top of Fig. 6. Next, we tried to increase the efficiency of velocity selection. Since signal and data handlings by computers and digital circuits were rapidly improving, time-of-flight (TOF) signals with different velocities of A* can be recorded at once as a series of time-resolved data in a time-resolution of 10^{-6} s order. Such TOF experiments were used earlier coupled with detection of produced ions.[70] However, for our purposes the TOF technique for velocity selection of A* should be combined with detection of Penning electrons. Here, it is important to note that the time resolution for TOF analyses of A* (10^{-6} s) is much shorter than the typical time scale for electron kinetic energy analyses (10^{-4} s). Thus, we decided to use the TOF technique for velocity selection of A* in combination of electron spectroscopy. For the TOF measurements we used a mechanical chopper rotating at 24000 rpm with a high-speed hysteresis synchronous motor (TRW Globe Motors, 18A1003-2). As shown in (2) in Fig. 6, this approach to velocity selection by TOF in combination with electronics and computers gave a signal increase of 2×10^3 times. We thus gained a total of 2×10^6 times improvement. This enabled us to make collision-energy resolved and ionic state resolved measurements of Penning ionization cross sections of molecules for the first time.[76,77] Thus, we arrived at the target stage of collision energy resolved measurements of PIES much earlier than 2019. However, it still took a long time, typically a few days, to perform these experiments, because two-parameter measurements for collision energies E_c and electron energies E_e should be made while repeating TOF measurements with point-by-point changes of E_e in the electron spectrometer by hand. The next project then aimed at developing full-automated collision-energy/electron-energy resolved two-dimensional Penning ionization spectroscopy (2D-PIES). An obstacle of this project was use of large amounts of computer memories for the 2D data. In 1988 when we first measured collision-energy dependence of partial Penning ionization cross sections (CEDPICS), a multi-channel scaler larger than 1 MB

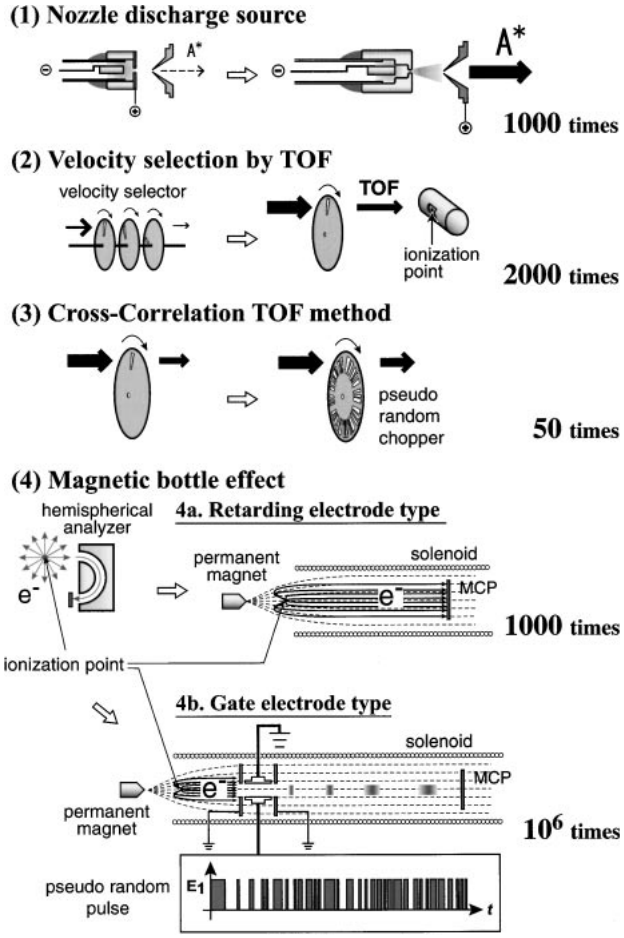

Fig. 6. Development of various parts of the collision-energy resolved Penning ionization electron spectroscopy apparatus. In the left sides, standard methods before the improvements are illustrated. In the middle, improved methods are schematically shown at the right of thick white arrows. Increased efficiencies of signal detection are listed on the right hand sides of the individual improvements.

was not available. In 1992 we noticed that 2 MB memories can be used, and we collaborated with Laboratory Equipment Corporation to construct a new 2 MB-multichannel scaler LN6600 at a time resolution of 1 μs. Electron energies were scanned by a step of 10 meV at a typical dwell-time of 30 ms, and the electron-energy scan was repeated for a typical recording time of a few hours. Two-dimensional signals were stored in a 2 MB random-access memory consecutively. With this new apparatus, we could observe 2D-PIES for the first time.[79] This 2D-PIES technique not only provides CEDPICS but also collision-energy-resolved Penning ionization electron spectra (CERPIES) from one set of data. Then we noted that the single slit chopper is inefficient, because many A* atoms cannot be used for measurements. We applied the cross-correlation technique to TOF measurements with using a pseudo random chopper and Hadamard transformation.[85,86] We used a photo-etched pseudo random pattern of 127 elements on a 104-mm diameter and 0.2 mm thick brass disk. This modification gained a further signal increase of ca. 50 times ((3) in Fig. 6).[80] It is of note that this cross-correlation technique

was also supported by the rapidly improved qualities of data processing devices. The 2D-PIES technique has been applied to many systems, and observed CEDPICS and CERPIES have been discussed in connection with anisotropic interaction potentials and stereo reaction dynamics in the collisional ionization processes.[52,53,57,58,80,81,87–120] Some examples of 2D-PIES studies will be given in the subsequent sections.

Applications of Penning ionization electron spectroscopy to van der Waals clusters are expected to be interesting, because many aspects of their stereoelectronic properties have been eluded observation. However, number densities of a particular cluster species in typical experimental conditions are usually very low in comparison with the monomer component or a usual sample such as nitrogen gas, by a factor of 10^{-2}–10^{-3} or much less. In addition, by contrast with photoelectron spectroscopy, back ground gases outside the ionization center should be decreased to be low enough. Otherwise, the metastable beam may easily be quenched before reaching the ionization center. Thus, in order for one to apply PIES techniques to van der Waals clusters, (1) the number density of the sample cluster should be increased as much as possible with keeping the background pressure low enough to avoid the quenching loss of A* atoms by background gases, and (2) the sensitivity of the electron spectrometer should be increased considerably. For this purpose, we constructed a highly sensitive Penning ionization electron spectrometer combined with a supersonic crossed beam source for samples. In the usual method for electron spectroscopy with a continuous excitation source, a hemispherical electrostatic deflection type electron analyzer has been widely used. This type of electron energy analyzer gives very low electron collection efficiency, ca. 10^{-3} or much less. Thus, we introduced a 4π electron collection technique using an inhomogeneous magnetic field known as the magnetic bottle effect[121–124] in combination with a retarding electric field. The electron energy analyzer consists of a strong-field permanent magnet near the collision center, a guiding solenoid around the electron flight tube, and a series of retarding electrodes. Typical magnetic fields at the collision center and in the flight tube are ca. 800 and 6 G, respectively. Almost all electrons emitted around the collision center were collected by the magnetic bottle effect to be led to the retarding electrodes placed in the flight tube and detected by a dual microchannel plate (MCP) at the end of the tube. The electron energy spectra were obtained by differentiating the integrated electron signals recorded as a function of the retarding potential. Figure 7 shows a schematic diagram of our collision-energy-resolved crossed-beam PIES apparatus using the magnetic bottle electron analyzer with retarding electrodes. This magnetic bottle electron analyzer increased the signal collection efficiency of our PIES apparatus by a factor of 10^3 ((4a) in Fig. 6).[82,83,125] Owing to this considerable increase of the signal sensitivity of our apparatus, Penning ionization electron spectra of van der Waals clusters could be measured for the first time.[82,83,125] Unusually fast electrons with extra kinetic energies of 1–2 eV as compared to those expected for vertical ionization have been detected for Ar and Kr van der Waals clusters in collisions with $He^*(2^3S)$ atoms. These fast electrons were ascribed to autoionization into stable ionic structures via superexcited states embedded in the ionization continua, and unusual electrons can be considered to be related to an adiabatically ionized state to which a direct ionization process is almost forbidden because of a very small Franck–Condon factor. The crossed molecular beam apparatus equipped with the magnetic bottle electron analyzing system has been applied to van der Waals clusters and some organic molecules. Penning ionization electron spectra of CO_2 clusters have been observed for the first time.[126]

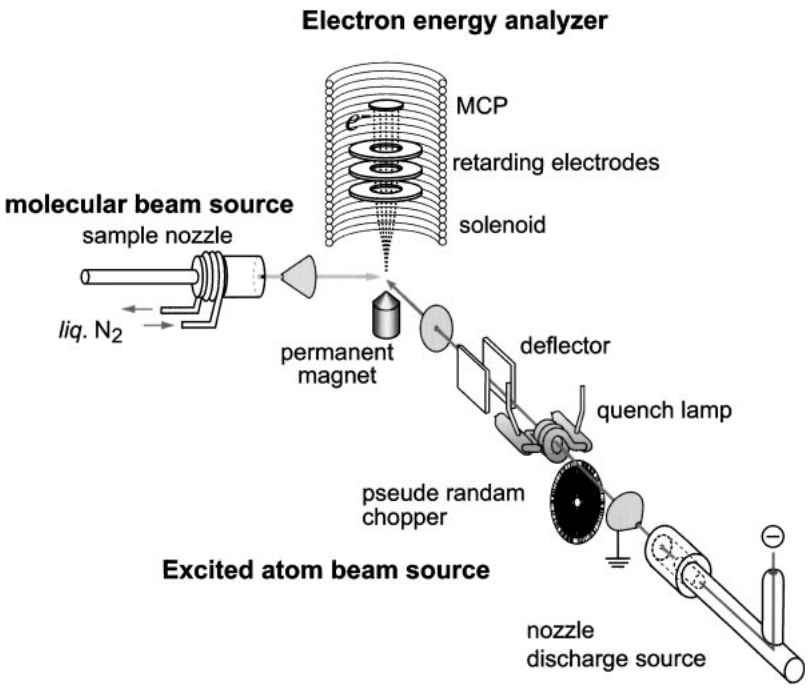

Fig. 7. Schematic diagram of the crossed-beam cross-correlation time-of-flight two-dimensional Penning ionization electron spectrometer equipped with a magnetic bottle retarding-type electron analyzer.

There still remain some inefficient parts in the experimental system. In our measurements electron kinetic energies were scanned gradually. If we can use a multiplex technique such as Fourier transformation spectroscopy, the signal sensitivity of PIES measurements will then be further increased by a factor of 10^2–10^3. We noted that the cross correlation method that has been used for modulation of metastable atom beams can also be applied to electron kinetic energy analyses. The important point is the time scale. In the case of atomic beams, their velocities are in the range of ca. 10^2–10^4 m s^{-1}, which requires a time resolution of ca. 10^{-6} s. On the other hand, electron velocities are very fast and ca. 6×10^5 m s^{-1} even for electrons of 1 eV. Thus a time resolution of ca. 10^{-9} s is needed for cross correlation experiments for electron beams. In view of recent development of the information technology in the GHz regions and even up to THz regions, we decided to attempt the construction of a multiplex electron energy analyzer. Although in the time resolution of 10^{-6} s we can use a mechanical chopper, it cannot be applied to electron beams in the time resolution of 10^{-9} s and in the corresponding frequency region of GHz. Thus, we used electric gates for chopping the electron beams. Preliminary but promising results were obtained.[127] Although our arbitrary pattern synthesizer is not fast enough, the forthcoming improvement of electronic devices will remove the difficulties to yield an excellent electron energy analyzer of a gate electrode type that only loses one half of electrons to be analyzed without scanning processes, which is ca. 10^6 times more efficient than the conventional hemispherical type electron energy analyzer ((4b) in Fig. 6). Since this electric gate electron energy analyzer can also be applied to various types of electron spectroscopic techniques using continuous excitation source, the following merits will be expected: (1) a drastic reduction of sample amounts, for example from 1 g to 1 μg, or (2) a dramatic reduction of measuring time by 10^{-6}, for example from 12 days to 1 s.

3. Trajectory Calculations for Penning Ionization and Interaction Potentials

In order to analyze experimental data on Penning ionization, classical trajectory calculations have been performed.[79,99,104,113,128–135] We will here briefly describe important aspects of the trajectory calculations.

The most important theoretical quantities of Penning ionization to be considered are the following three functions of the distance R between M and A* (or M^+ and A);[26]

(1) the interaction potential for the entrance channel (M + A*), $V_*(R)$,
(2) the interaction potential for the exit channel (M^+ + A), $V_+(R)$,
and
(3) the electronic transition rate $W(R)$ or the ionization width $\Gamma(R) = \hbar W(R)$.

All aspects of Penning ionization can be calculated by using these functions. The most important experimental quantities are the collision energy E_c and the ejected electron energy E_e. It should be noted that E_e is directly related with the difference of potential functions.

$$E_e(R) = V_*(R) - V_+(R). \tag{3}$$

For a particular trajectory of A* approaching to M with a collision energy of E_c and an impact parameter b, the transition probability can be calculated in the interval between R and $R + dR$ as $P_b(R)dR$ which is a sum of the incoming contribution of $P_b^{in}(R)dR$ and the outgoing contribution of $P_b^{out}(R)dR$;

$$P_b(R)dR = P_b^{in}(R)dR + P_b^{out}(R)dR. \tag{4}$$

For the incoming contribution, the probability is a direct product of the following three factors; the survival provability of A* in the excited state, $S_b^{in}(R)$, the transition rate, $W(R)$, and time spent at dR, $dR/v_b(R)$, where $v_b(R)$ is the relative velocity at R.

$$P_b^{in}(R)dR = S_b^{in}(R) \cdot W(R) \cdot dR/v_b(R). \tag{5}$$

The survival probability is related to $P_b^{in}(R)$ as

$$S_b^{in}(R) = 1 - \int_R^\infty P_b^{in}(r)dr. \tag{6}$$

For the outgoing contribution, the probability is given similarly:

$$P_b^{out}(R)dR = S_b^{out}(R) \cdot W(R) \cdot dR/v_b(R), \tag{7}$$

$$S_b^{out}(R) = 1 - \int_{R_0}^\infty P_b^{in}(r)dr - \int_R^{R_0} P_b^{out}(r)dr, \tag{8}$$

where R_0 is the shortest distance at the turning point of the trajectory. Results for various values of b with a given E_c should be integrated, and then the probability function $P(R)$ for a particular E_c can be obtained.

$$P(R) = 2\pi \int_0^\infty P_b(R)bdb. \tag{9}$$

The distance dependence of the transition probability $P(R)dR$ can be related to the probability of electron ejection with an energy between E_e and $E_e + dE_e$,

$$P(E_e)dE_e = P(R)dR. \tag{10}$$

Here, dE_e/dR is related with potential functions by Eq. 3. A set of these calculations for various E_c values yields $P(E_e, E_c)$, which provides a theoretically synthesized 2D-PIES. Once a theoretical 2D-PIES is calculated, CERPIES can be obtained by fixing E_c at a given collision energy or by partially integrating $P(E_e, E_c)$ in a certain range of E_c, and also CEDPICS can be obtained by partial integration of $P(E_e, E_c)$ for a particular ionic state with a certain range of E_e values.

Although the outline of the above procedures is simple for atomic targets, there have been many obstacles to perform such calculations for molecular targets. First of all, molecular systems are in general highly anisotropic different from atomic systems. Thus, geometrical situations cannot be described by a single coordinate of the distance R and an initial condition of the impact parameter b. The molecular orientation as well as the direction should be considered throughout the collision processes. These features make it very difficult to construct potential energy functions both for entrance and exit channels. To make the matter worse, molecular targets have in general many ionic states for the exit channels. It is well known that the full construction of potential energy surfaces becomes almost impossible when the system contains more than three atoms. It should also be noted that calculations of excited-state potential

energy surfaces are in general much more difficult than calculations of the ground-state potentials. Starting with an atomic target of Ar[79] and a simple molecular target of N_2,[128] we have developed a model potential approach based on quantum chemical calculations. In this connection, we have also developed various mathematical treatments utilizing interpolation techniques, non-linear optimization methods, and numerical calculation methods, as described below.

Entrance potentials V_* involving electronic excited states embedded in ionization continua are very difficult to determine. Huge numbers of electronic configurations should be considered, because molecular ionization energies are much lower than the excitation energy of the A* atom. It has been established that interaction potentials between A* and various targets can be approximated by replacing A* by the respective alkali atom with the same electron configuration in the valence shell.[136–138] This model seems to be natural, because interaction potentials are mainly related with the outermost electrons. Thus, a Li 2^2S atom can be used in place of a He* 2^3S atom, and then a model potential V_0 is obtained for the entrance potential V_*. Because of the approximate nature of Li–M potentials V_0, the subsequent techniques using semiempirical parameters have been introduced to optimize V_* based on V_0. In order to obtain a suitable V_0 by ab initio methods, it is important to use basis sets with diffuse functions and also to include electron correlation effects. In our earlier studies, we used the second order Møller–Plesset perturbation theory with 6-311+G* basis set for N_2.[128] Recently, we performed CCSD(T) calculations with 6-311++G** basis sets for C_2H_2.[134]

(Simple Scaling Method)

In order to modify the bare Li model potential, the following simple scaling (SS) model was introduced:

$$V_*{}^{SS} = cV_0. \tag{11}$$

Here, c is a scale factor that is determined so as to reproduce observed PIES data. This simple scaling method has only one adjustable parameter, and thus the optimization process is straightforward. This method was applied to some linear molecules, such as N_2[128,130] and CO.[104] Although the results were found to be satisfactory, some inaccuracy remained for CO. Since potentials for CO–He* are more anisotropic, the simple scaling procedure cannot correct the difference between the oxygen side and the carbon side. Moreover, this method cannot be applied to molecular systems with deep potential wells, because adjustments for positive parts and those for negative parts are contradicting.

(Exponential Correction Method)

In order to overcome some drawbacks in the simple scaling method we introduced the following exponential correction (EC) method:

$$V_*{}^{EC} = V_0 - \Sigma_i A_i P_i(\cos\theta)\exp(-R/B). \tag{12}$$

Here, R is the distance between the He*(Li) atom and the center of mass (CM) of the molecule, θ denotes the angle of the position vector **R** directing to the He*(Li) atom from the CM with respect to the molecular axis, $P_i(\cos\theta)$ is the i-th order term of Legendre polynomials, and A_i and B are parameters to be optimized. This method was found to be satisfactory for N_2 and CO,[131] though the convergence in the optimization processes becomes very slow when the higher order terms ($i > 4$) in the Legendre expansion are taken into account.

(Overlap Correction Method)

In order to make meaningful corrections to the bare Li potential V_0, the following overlap correction (OC) model was proposed:[134]

$$V_*{}^{OC} = V_0 - \Sigma_i C_i |\langle\phi_i|\chi\rangle|^2, \tag{13}$$

$$\chi = \sqrt{\zeta^3\pi^{-1}}\exp[-\zeta r]. \tag{14}$$

Here, χ is a Slater-type atomic orbital function at the position of the He*(Li) atom, ϕ_i is the i-th molecular orbital, and C_i and ζ are parameters to be optimized. This model is based on the consideration that the difference between Li and He* atoms will be compensated by interactions of an s-type atomic orbital with the target molecular orbitals, which may be approximated by their overlap integrals. This OC method has been found to be more efficient in the optimization procedures than the EC method using the Legendre expansion, because the highly anisotropic nature and most important interactions with the frontier orbitals are effectively taken into account.[133–135] In a recent study to determine the potential well for benzene–He*(2^3S), the OC method gave accurate results of ±10 meV and ±0.06 Å.[135]

Energies of the exit potentials $V_+{}^{(i)}$ for the i-th ionic state of the target molecule M interacting with a ground state He atom can be calculated by several ways. The absolute value of an orbital energy can be treated as the respective ionization energy IE based on the Koopmans' theorem.[7] This method is referred to as HF. The second method is to obtain IE values by the outer valence Green's function method (OVGF) in which many body effects are included.[139,140] In these HF and OVGF methods, the potential energy function for the i-th ionic state $V_+{}^{(i)}$ can be expressed as the summation of the neutral potential for the ground state V_G and the respective ionization energy $IE^{(i)}$, $V_+{}^{(i)} = V_G + IE^{(i)}$. The third method is multi-reference single and double excitation configuration interactions (MRSDCI). These methods were compared for the ionic states of He + N_2[130] and He + CO.[104] Electron correlation effects on V_+ were found to be of unexpectedly minor importance. Even the HF method gave good potential surfaces, though the absolute magnitude should be adjusted to the observed values. This is probably due to electrostatic interactions between a molecular ion and a neutral He atom being dominant. The OVGF method was found to be comparable with the MRSDCI method, for the ionic-state potential surfaces of He + N_2 and He + CO. Thus the ionic state potential between a rare gas atom and a molecule can be constructed in an economic way by using the ionization energies in combination with neutral potentials between the atom and the molecule in their ground states. Analogous treatments were also recently reported for ionic clusters of He–CO^+, Ne–CO^+, and Ar–CO^+.[141]

The imaginary part of the entrance potential, $-i\Gamma/2$, is related to the ionization width $\Gamma^{(i)}$ for the i-th ionic state, which is given by

$$\Gamma^{(i)} = 2\pi\rho^{(i)}|\langle\Phi_0|H_{el}|\Phi^{(i)}\rangle|^2. \tag{15}$$

Here, $\rho^{(i)}$ is the density of final states, H_{el} is the electronic Hamiltonian, and Φ_0 and $\Phi^{(i)}$ are electronic wave functions for the initial and the i-th final states, respectively. The dependence of

$\Gamma^{(i)}$ on the distance R was assumed as $A\exp(-BR)$ in many earlier studies.[26,142–145] However, for molecular target systems both A and B are highly anisotropic, in addition to having extra R-dependence. Recent calculations for Ar with $He^*(2^{1,3}S)$ showed that ionization widths deviate from the single exponential form.[146] Since the R dependences of directly calculated $\Gamma^{(i)}$ for N_2[147] were very similar to those of the overlap integrals, we arrived at the following treatments. Slater determinant wave functions composed of one-electron orbitals for both initial and final states lead to the next formula for the integral in Eq. 15:

$$\langle\Phi_0|H_{el}|\Phi^{(i)}\rangle \approx \langle\psi_{2s}(1)\phi_i(2)|{r_{12}}^{-1}|\psi_{1s}(1)\phi_\varepsilon(2)\rangle - \langle\psi_{2s}(1)\phi_i(2)|{r_{12}}^{-1}|\psi_{1s}(2)\phi_\varepsilon(1)\rangle, \quad (16)$$

where ψ_{2s} and ϕ_i are the 2s orbital of He^* and the i-th orbitals of the target molecule in the initial states, respectively, and ψ_{1s} and ϕ_ε are the He 1s orbital and the outgoing ejected electron orbital in the final state, respectively. For $He^*(2^3S)$, the first term vanishes due to the spin inversion. The remaining second term in Eq. 16 can then be approximated as a product of two overlap integrals

$$C\langle\phi_i|\psi_{1s}\rangle\langle\psi_{2s}|\phi_\varepsilon\rangle, \quad (17)$$

C is a constant factor obtained by replacing r_{12} with a suitable average value.[148] This overlap approximation is based on the Mulliken approximation[149] for the two electron integral $\langle st|uv\rangle$.

$$\langle st|uv\rangle = (1/4)\langle s|u\rangle\langle t|v\rangle\{\langle ss|tt\rangle + \langle ss|vv\rangle + \langle uu|tt\rangle + \langle uu|vv\rangle\}. \quad (18)$$

Such an approximation has been extensively used in semiempirical molecular orbital theories as well as in semiempirical treatments for electron transfer rates in various electron transport phenomena including charge transfer[150] and exciton diffusion.[151] Because the He 2s orbital and the outgoing electron orbital are very diffuse, anisotropy of the ionization width is governed by the compact He 1s orbital and the ionized molecular orbital. Thus, the following formula can be used for the ionization width:

$$\Gamma^{(i)} = K^{(i)}|\langle\phi_i|\psi_{1s}\rangle|^2. \quad (19)$$

$K^{(i)}$ can be determined in order to reproduce observed branching ratios and total ionization cross section. It should be noted that, if we perform direct calculations of two electron integrals without using the Mulliken approximation, computational demands for trajectory calculations will easily exceed the available range of the computing system both for storage space and computation time. It is also of note that, if the overlap integral in Eq. 19 is replaced by a single exponential function, we then obtain $\Gamma = A\exp(-BR)$, which is the widely used simple formula.[26,142–145] The overlap approximation in Eq. 19 takes into account anisotropic parts of target wave functions as well as their radial dependence.

In order to obtain potential energy surfaces based on quantum chemical calculations, we should consider computation time and amounts of data. We need $V_*(R)$, $V_+(R)$, and $\Gamma(R)$ at an arbitrary geometry of the reaction system. If calculations obtaining these functions are very simple, we might perform them at any position of each trajectory. However, costs of quantum chemical calculations for the above functions are very high in comparison with classical treatments of trajectories. Moreover, we need to perform about 10^4 trajectory calculations for statistical treatments. Thus, we need to reduce computational demands on quantum chemical calculations for $V_*(R)$, $V_+(R)$, and $\Gamma(R)$. This is one of the important reasons why we introduced overlap approximation for $\Gamma(R)$ instead of direct calculations of two electron integrals and also why we used model potentials for $V_*(R)$. Discovery of the unexpectedly good qualities of the OVGF and HF calculations for $V_+(R)$ makes it easier to use them rather than to use the much more demanding calculations of MRSDCI.

For a drastic reduction of quantum chemical calculations, interpolation techniques need to be used; the energy for an arbitrary point on a potential energy surface (PES) can be created by interpolation of stored data for limited numbers of points on the PES. For this purpose we have developed the following method. Potential data are interpolated with cubic spline functions to obtain the potential energy at arbitrary orientation of the He atom and a molecule. In order to obtain the maximum efficiency to reduce essential data points as well as to minimize inaccuracies associated with interpolations, one should employ the following procedures: (1) At first, spline treatments are taken along radial directions from the center of mass of the molecule, since the asymptotic properties at the shorter and the longer distances are expected to be very simple. At very shorter distances, the exchange repulsion is very large, and hence the radial dependence is expected to be simply decreasing like an exponential function. At the very longer distances, the interaction energies should simply vanish. (2) In the second step, spline treatments are made for circular directions along with circles of suitable radii for which potential values at crossing points with radial axes could easily be obtained from the splined data determined in the first step. (3) Potential values at arbitrary points are obtained from the splined data in the first two steps at every instance of trajectory calculations; a radial spline along a direction including the sampled point is performed by using already determined circular spline curves for various radii to yield the potential value of the sampled point very efficiently. It should be noted here that if one uses rectangular lattice points, hundred times of additional points would be required to obtain smooth and precise results of the interpolation. Our polar coordinate cubic spline technique has been found to be very efficient and satisfactory.

In order to increase the efficiency of our trajectory calculations, we used the following techniques. In order to determine classical trajectories, differential equations are solved numerically by the fourth-order Runge–Kutta method with adapted step size control.[152] Although in a real trajectory the ionization event occurs at most once at a certain position on that trajectory, one may treat a bundle of the same trajectories in a statistical way for computational efficiency. The integrated partial ionization probability can also be treated as a function of time (or positions): it can be determined by integration of partial ionization probability values before time t (or before arriving at the position). Then, the survival factor can be obtained from the summation of the partial ionization probability values over the possible ionic states. The transition rate to the i-th ionic state for this particular bundle of the same trajectories can then be evaluated with the ionization widths $\Gamma^{(i)}$ at each geometrical config-

urations of He^* and a molecule. In the optimization procedures of our model potentials, we employed an efficient nonlinear least squares method. Although this method is basically a modified Marquart method,[152] gradients are efficiently renewed from the current data in our calculations. It should be stressed here that various technical developments and improvements have been necessary to make it possible to perform highly demanding computations in efficient ways.

4. Comparison of Observed 2D-PIES and Trajectory Calculations

Comparison of observed 2D-PIES and trajectory calculations allowed us to determine entrance potentials V_* of M + $He^*(2^3S)$ for various systems. Optimization of model potentials were made by adjusting parameters in the models to minimize discrepancies between observed and calculated CEDPICS and branching ratios (relative band intensities in CERPIES).[132–135]

Figure 8 shows (a) observed and (b) calculated two-dimensional Penning ionization electron spectra for $N_2 + He^*(2^3S)$. Heights of electron signals or cross sections are shown in a relative unit. The right-hand panel of each figure shows CERPIES drawn with a solid line for $E_c \sim 100$ meV and with a dotted line for $E_c \sim 300$ meV. Figure 9 shows $\log \sigma^{(i)}$ vs $\log E_c$ plots of CEDPICS for $N_2 + He^*(2^3S)$, $CO + He^*(2^3S)$, and $C_2H_2 + He^*(2^3S)$. Observed cross sections are plotted with circles, and they are compared with those for calculations shown with solid lines. Contour maps of the electron densities for molecular orbitals corresponding to the respective ionic states are also shown in Fig. 9, in which the thick solid line in the maps shows the contour curve of 800 meV of the entrance potential as a reference of the repulsive boundary. In the maps of the molecular orbitals and the repulsive boundary, the thick arrow indicates important directions of the interactions between the molecule and the He^* atom. The most reactive directions are in the perpendicular directions for Π states and the collinear directions for Σ states, reflecting the respective orbital electron distributions. It is of note that, for the Π state (A) of $N_2 + He^*(2^3S)$, the most reactive directions change from ca. 50° to 90° from the collinear direction on going from 100 to 400 meV. This unusual behavior is related to the dramatic change of the outer shape of the boundary surface for N_2 with $He^*(2^3S)$ from the oblate form to the prolate form with increasing energies, which will be shown in the next section. Intensities of A state for both $N_2 + He^*$ and $CO + He^*$ increase more rapidly with the increase of E_c than those of X or B state. This difference reflects the softness of the repulsive potentials towards perpendicular directions of molecular axis in the collision energy range of the present study. CEDPICS for X and B states (Σ states) are nearly the same for $N_2 + He^*$, because the electron distributions of respective σ orbitals ($3\sigma_g$ and $2\sigma_u$) are very similar in the collinear directions ($\theta = 0°$). In the case of $CO + He^*$, CEDPICS for X and B states (Σ states) are on the other hand considerably different, because of the difference of the electron distribution of the corresponding σ orbitals (5σ and 4σ; the exterior electron distribution is dominant at the C-atom side ($\theta = 0°$) for 5σ orbital and at the O-atom side ($\theta = 180°$) for 4σ orbital. Since the repulsive wall for $\theta = 0°$ is much more

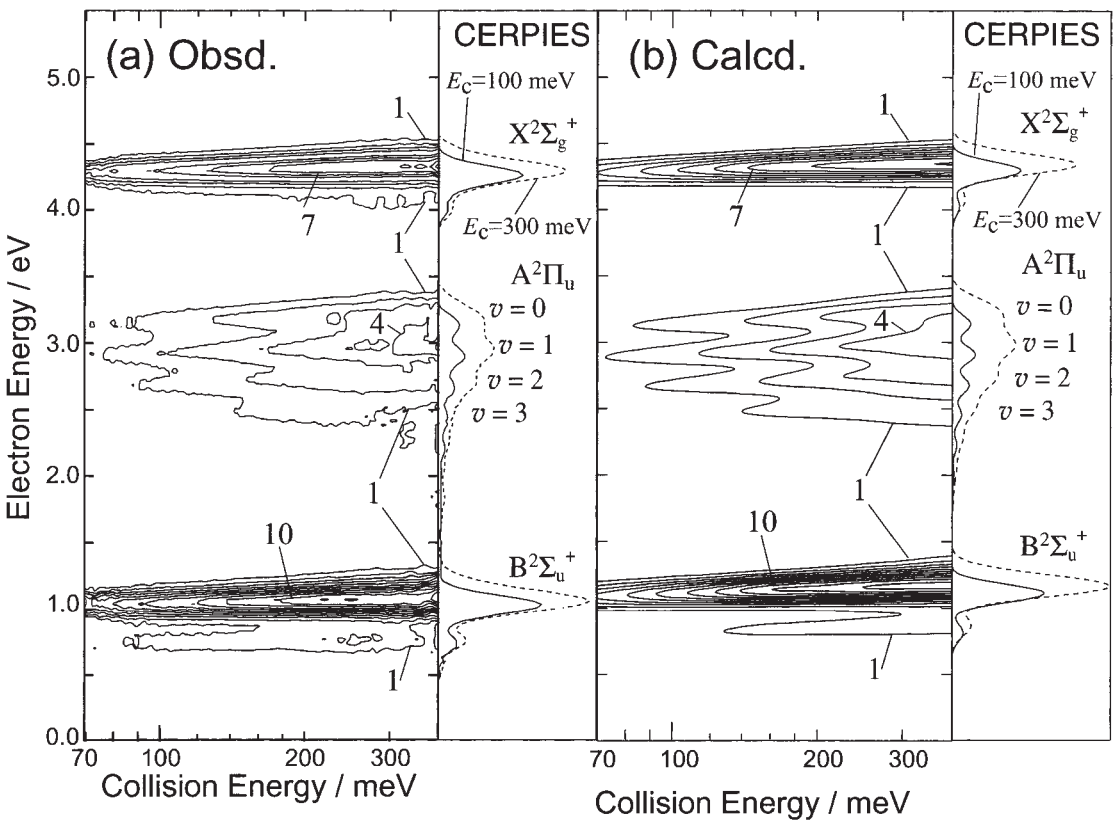

Fig. 8. (a) Observed and (b) calculated two-dimensional Penning ionization electron spectra (2D-PIES) for $N_2 + He^*(2^3S)$. The right hand panel shows CERPIES for collision energies of 100 and 300 meV.

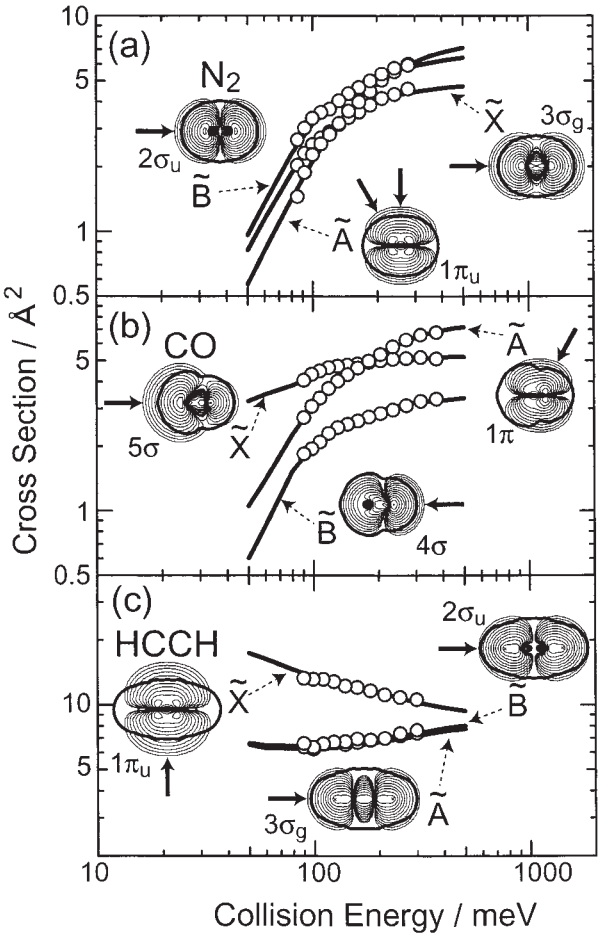

Fig. 9. The $\log \sigma^{(i)}$ vs $\log E_c$ plots of CEDPICS for (a) N_2 + $He^*(2^3S)$, (b) CO + $He^*(2^3S)$, and (c) C_2H_2 + $He^*(2^3S)$. Observed cross sections are plotted with circles, and calculated curves are drawn with solid lines. Contour maps of the electron densities for molecular orbitals corresponding to the respective ionic states are also shown.

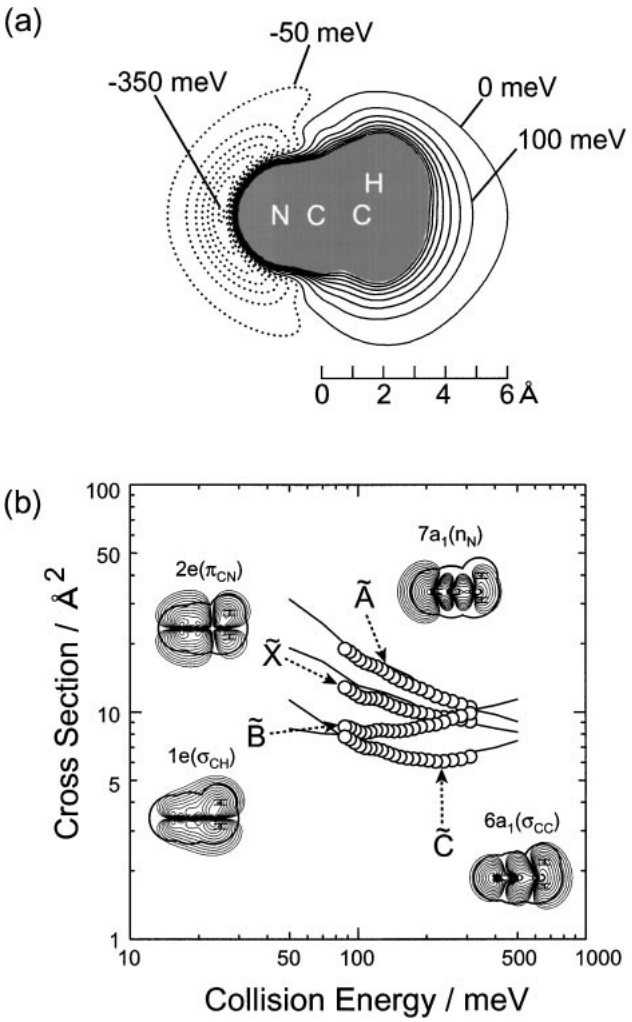

Fig. 10. (a) The contour map of the potential energy surface V_* and (b) the $\log \sigma^{(i)}$ vs $\log E_c$ plots of CEDPICS for CH_3CN + $He^*(2^3S)$. A cutting plane is taken for the molecular three-fold axis. The spacing of the contour curves is 100 meV for positive parts and 50 meV for negative parts.

hardened than that for $\theta = 180^\circ$ in the energy range between 180 and 40 meV, the slope of the CEDPICS for X state of CO^+ is more flattened.

Figures 10 and 11 show $\log \sigma^{(i)}$ vs $\log E_c$ plots of CEDPICS for CH_3CN + $He^*(2^3S)$ and C_6H_6 + $He^*(2^3S)$, respectively. Obtained potential energy surfaces are also shown in these figures. Positive contours corresponding to repulsive surfaces show the softness; (1) the surface is hard where the interval is close, and (2) the surface is soft where the interval is wide. Hydrogen regions are rather hard in comparison with the C atoms or the CC bond area. In the negative regions, a deep and wide potential well causes strong attractive or adhesive effects. The nitrogen lone-pair region around CH_3CN is very strongly adhesive with a He^* atom. The π electron regions of benzene are rather weak but widely adhesive with a He^* atom. This is interesting, because strong affinities of alkali metal atoms with π electron systems are well known.

5. Exterior Characteristics of Molecular Surfaces Probed by $He^*(2^3S)$ Atoms

On the basis of 2D-PIES and trajectory calculations, exterior characteristics of molecular surfaces probed by $He^*(2^3S)$ atoms have been elucidated. The qualitative nature of molecular surfaces with $He^*(2^3S)$ atoms can be classified into repulsive (r) or attractive (a) from the positive or negative slope observed in CEDPICS, as shown in Fig. 5. Slope values m for $\log \sigma^{(i)}$ vs $\log E_c$ plots of CEDPICS have been measured for various systems. Table 3 lists the (r) or (a) characteristics of local regions on molecular surfaces probed by $He^*(2^3S)$ atoms and typical slope values m for collision energy ranges of 100–200 meV in parentheses. Types of molecular orbitals and the most relevant atoms are listed with the surface characters and references.

Figure 12 shows the principal orbital interactions between a He^* atom and a target molecule M. The major factor of bonding interactions that may lead to production of an attractive potential well causing adhesive forces is related to the interaction of the 2s electron in He^* with occupied electrons in the molecule M, which is specified as **1** in Fig. 12. However, the orbital interaction denoted as **1*** in Fig. 12 deteriorates the bonding characters by the unpaired electron. On the other hand, contributions of the 2p orbital of He^* (**2**) as well as an unoccupied

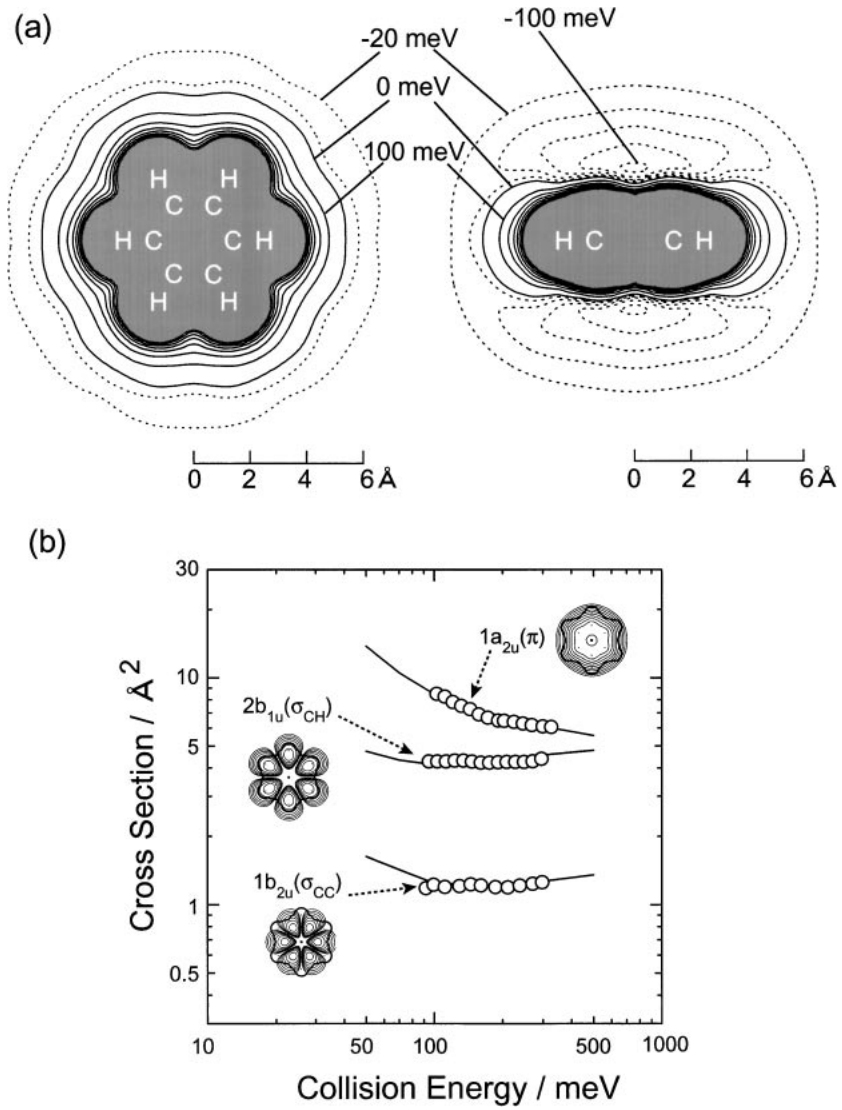

Fig. 11. (a) The contour map of the potential energy surface V_* and (b) the $\log \sigma^{(i)}$ vs $\log E_c$ plots of CEDPICS for C_6H_6 + $He^*(2^3S)$. Cutting planes are taken for the molecular plane and a plane including the six-fold axis. The spacing of the contour curves is 100 meV for positive parts and 20 meV for negative parts.

orbital of M (**3**) may considerably reduce the antibonding nature of the unpaired electron. It should be noted that the anisotropic nature of the interaction potentials is due to the electron distribution of target molecular orbitals via orbital interactions **1** and **3**. Figure 13 demonstrates the importance of the orbital interaction **1**; the magnitude of the slope m in CEDPICS for HOMO shows a correlation with the height of the HOMO energy levels.[93] A similar tendency has also been confirmed for a comparison of paracyclophane with benzene; the former has the higher occupied π levels and the larger negative slope in CEDPICS than the latter.[53] Attractive potential wells are located around lone-pair electrons and CX (X = C, N, O, S) double bonds with π electrons, which is consistent with (1) high electron densities in the exterior regions and (2) high MO energy levels or low ionization energies.

In connection with the above tendencies, repulsive characteristics of molecular surfaces have been found for N_2, CO, H_2, which have rather high ionization energies of 14–16 eV, which result in low occupied orbitals leading to very weak interactions for **1**. Around H atoms in hydrocarbon molecules, repulsive potentials are dominant, because σ_{CH} orbitals have localized electron distribution in the interior bonding regions and rather high ionization energies (ca. 13–16 eV). Combinations of orbital interactions **1** and **3** are most effective for σ orbitals in collinear geometries, whereas for π orbitals the interaction **3** cannot occur because the unoccupied orbital has a nodal plane in the perpendicular directions where π electrons are distributed.

The sp hybridization in the interaction **2** can also contribute more effectively for σ_{XY} type orbitals, when the outside atom Y is more electronegative than the inside atom X. As can be seen from Fig. 12, the sp hybridization on He^* atom causes an electric polarization with the negative side in the outward direction, which has a strong attractive interaction with the bond-dipole of $X^{\delta+}Y^{\delta-}$. Such types of very strong attractive interactions were found for σ_{CO} orbitals of carbonyl compounds and σ_{CN} orbitals of nitrile compounds. The σ_{NC} orbital in CH_3NC shows much less attractive interactions than the σ_{CN} orbital in CH_3CN be-

Table 3. Repulsive (r) or Attractive (a) Characteristics of Local Regions on Molecular Surfaces Probed by $He^*(2^3S)$ Atoms

Type	Atom	Character (m)	Reference
π_{NN}	N	r (soft)	77, 81, 128, 130, 132
σ_{NN}	N	r (hard)	77, 81, 128, 130, 132
π_{CO}	C, O	r (soft)	104, 132
σ_{OC}	C	r (hard)	104, 132
σ_{CO}	O	r (medium)	104, 132
σ_{CH}	H	r (0.1–0.4)	78, 87, 88, 89, 90, 80, 95
σ_{CO}	O	a (−0.2 to −0.5)	87, 89, 100, 101, 105
σ_{CN}	N	a (−0.2 to −0.5)	87, 90, 94, 80, 111, 119, 120
σ_{NC}	C	a (−0.087)	90
σ_{CS}	S	r, a (0.014 to −0.24)	87, 117
σ_{NO}	O	a (−0.78)	98
σ_{CF}	F	a (−0.1 to −0.5)	107, 108
n_F	F	a (−0.2 to −0.3)	106, 107
n_{Cl}	Cl	a (−0.1 to −0.3)	88, 97, 106, 108, 109, 114, 118
n_{Br}	Br	a (−0.3 to −0.4)	106, 115, 118, 120
n_I	I	a (−0.3 to −0.4)	97, 106, 119
n_O	O	a (−0.1 to −0.3)	89, 91, 92, 57, 95
n_S	S	a (−0.2 to −0.6)	92, 57, 101, 103, 117, 133
n_N	N	a (−0.2 to −0.6)	92, 94, 98, 100, 102
π_{CC}	C	a (−0.1 to −0.6)	78, 89, 93, 80, 97, 53
π_{CN}	N	a (−0.2 to −0.5)	90, 92, 94, 80, 111
π_{CO}	O	a (−0.2 to −0.4)	87, 89, 92
π_{CS}	S	a (−0.1 to −0.3)	87, 92

Typical slope values m are listed in parentheses.

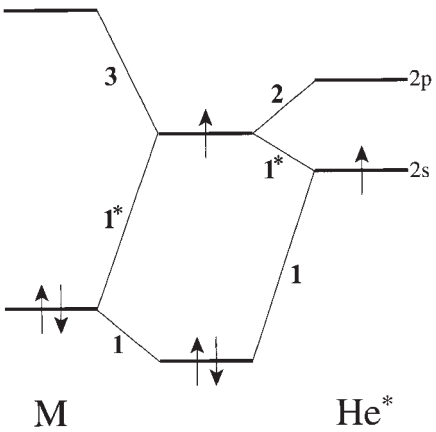

Fig. 12. Orbital interactions between a molecule M and a $He^*(2^3S)$ atom. The axis for the 2p orbital is taken to be directed to M.

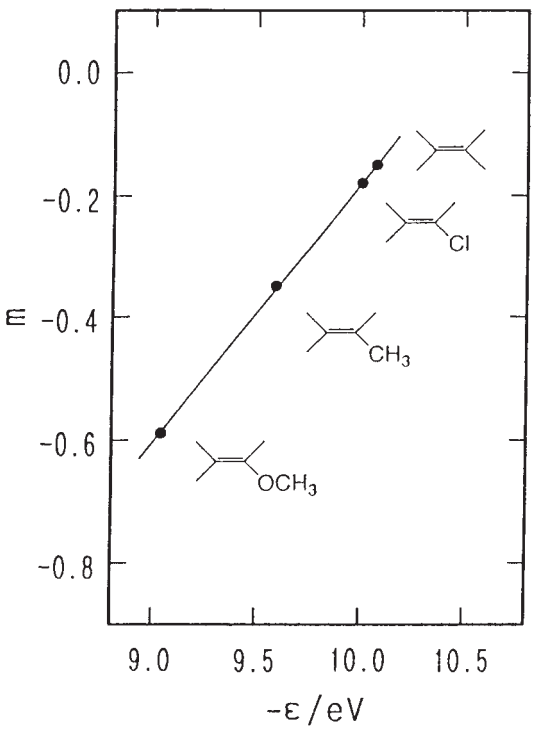

Fig. 13. Slope values m in CEDPICS against orbital energies of HOMOs for ethylene, vinyl chloride, propene, and methyl vinyl ether.[93]

cause of the reversed electro-negativities.[90] It should also be noted that the C=S group[87,117] gives much less attractive interactions than the C=O group. Figure 14 demonstrates that attractive interactions around an S atom occur in different directions in comparison with those around an O atom;[133] the collinear side around the O atom is very attractive, whereas the collinear side is rather repulsive around the S atom. Relative orders of IE for C, S, and O atoms are IE(O) > IE(C) > IE(S). Thus, the above mechanism leading to the bond polarization is not effective for the C=S group in a collinear geometry. On the other hand, high HOMO levels of degenerate nonbonding 3p orbitals directed vertical to the C=S axis yield strong attractive interactions in perpendicular directions. Similar anisotropic interactions were also found for a comparison of F and other halogen atoms;[106–108] an attractive potential well is located along the CF axis in C_2H_5F, whereas in C_2H_5Cl the attractive well is sur-

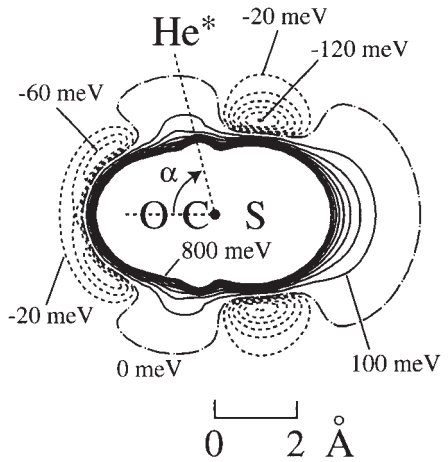

Fig. 14. Anisotropy of attractive potential well around S and O atoms in OCS. The spacing of the contour curves is 100 meV for positive parts and 20 meV for negative parts.

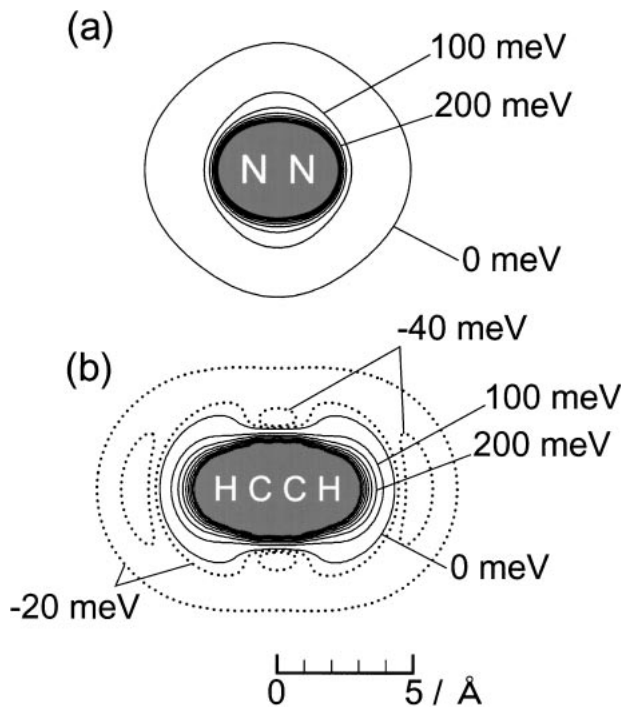

Fig. 15. Outer shape of (a) N_2 and (b) C_2H_2 probed by a $He^*(2^3S)$ atom. The spacing of the contour curves is 100 meV for positive parts and 20 meV for negative parts.

rounding the CCl bond.[108] The bond polarization effects, which are very important for the first row atoms of N, O, and F, were found to be negligibly small for the lower row atoms such as S, Cl, Br, and I.

6. Outer Shape of Molecules as Probed by Atoms

Based on experimentally determined interaction potentials V_* of M + $He^*(2^3S)$ for various target molecule M, the outer shape of molecules probed by $He^*(2^3S)$ atoms can be shown as contour curves for certain constant potential energies. Some interesting examples are shown in Fig. 15.

Figure 15(a) shows the outer shape of N_2 probed by $He^*(2^3S)$ atoms. Contour lines are drawn from 100 to 800 meV with a constant spacing of 100 meV. Contour curves for energies larger than 800 meV are not shown, because they almost overlap with the curve at 800 meV. Interesting features of this example can be summarized as follows.

The shape depends on the energies, since the outer boundary is not rigid as the simple VDW model. At the higher energy limit, the outer shape can be represented by the curve at 800 meV, which seems to be consistent with our common notion that the length along the NN axis is much larger than the diameter for the vertical direction. However for the lower energies, the shape gives a dramatic change into an unbelievable form that the NN axis is shorter than the diameter. The intervals between the contour curves change with the energies. This means that the softness of the repulsive molecular surface changes dramatically. Narrow intervals mean steep repulsive walls, giving hard repulsion. Wide intervals, on the other hand, indicate small inclinations of the repulsive slope, leading to soft repulsion.

Figure 15(b) shows the outer shape of C_2H_2 probed by $He^*(2^3S)$ atoms. Contour lines are drawn from 100 to 800 meV with a constant spacing of 100 meV for positive parts: for negative parts, contours are shown with a spacing of 20 meV. This example also demonstrates that the shape and the softness of the molecular surface depend dramatically on the energies. Of course, at the higher energy limit, the shape looks very similar to our common image of the molecular shape for C_2H_2, which has larger diameters at C atoms than at H atoms, in good agreement with the VDW model. However for the lower energies, sizes of the atoms in the molecule become reversed; H atoms show much larger boundaries than C atoms in contradiction with our common knowledge about the C_2H_2 molecule.

Unusual characteristics in the molecular shapes at lower energies have been understood from anisotropic interactions pulling down the potentials.[77,153,154] As has been discussed in connection with orbital interactions in Fig. 12, special directions undergoing the pulling down effects of the repulsive walls are (1) for N_2 in the collinear directions along the molecular axis around lone pair regions and (2), on the other hand, for C_2H_2 in the vertical directions around π electron regions.

Although experimental studies on molecular surfaces are not so easy, theoretical calculations may be applied to this problem much more systematically. We have obtained ab initio isopotential energy contours of some simple molecules probed by test atoms from H to Ar.[153,154] Ab initio quantum chemical calculations were performed with sufficient sizes of basis functions, and full counterpoise corrections were made to avoid basis-set superposition errors. The molecular skeletons were fixed at their equilibrium structures, because the general characteristics of the shapes were found to be nearly the same even if optimized structures were used.

Figure 16 shows ab initio energy contours of (a) $H_2(^1\Sigma_g^+)$ and (b) $N_2(^1\Sigma_g^+)$ by single test atoms from H to Ar in the ground states. Interesting features of molecular shapes in Fig. 16 can be summarized as follows: (1) prolate forms elongated along the diatomic axis are found for many cases in consistent with the VDW models; (2) in some cases the lengths

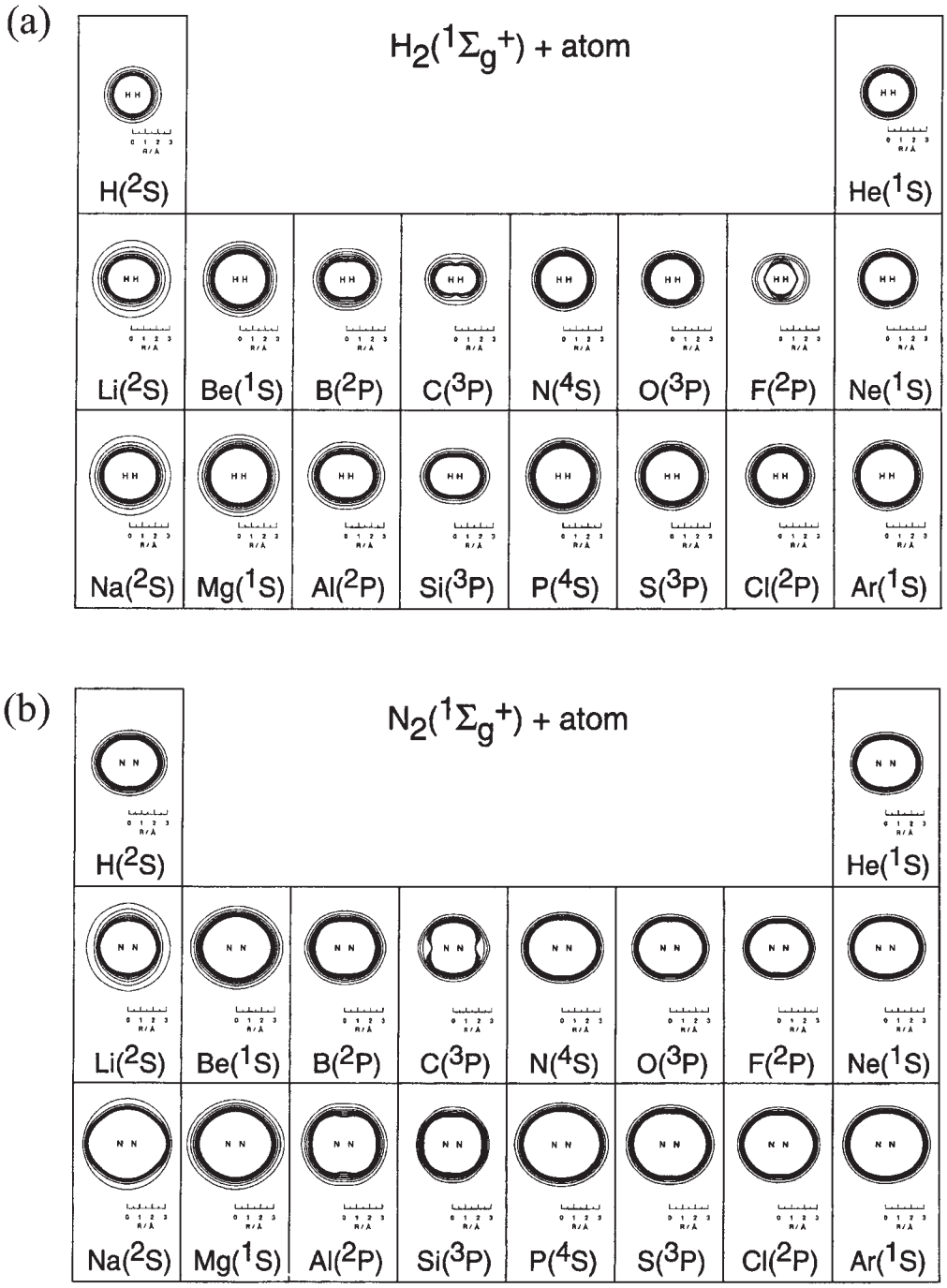

Fig. 16. Ab initio isopotentail energy contour of (a) H_2 and (b) N_2 by a test atom from H to Ar in the ground state.[153]

along the diatomic axis are shortened to become a sphere form or even an oblate form; (3) some other cases exhibit dented structures along certain directions to yield an apple form, a peanut form, and a lemon form. These prototypes are illustrated in Fig. 17. Although shapes depend on the probing atom, this does not indicate that the probed shape should be ascribed to the probing atom. As can be seen in Fig. 16, the dented structures are different for H_2 and for N_2 for the same probing atom of $C(^3P)$. In the case of H_2 + C, the dented part appears in the vertical directions to lead to a peanut form, while in the case of N_2 + C the axial directions are dented to give an apple form. Somewhat strange characteristics of the outer molecular shapes can be ascribed to anisotropic interactions between a molecule and an atom. Repulsive surfaces become dented, when anisotropic interactions reduce repulsion around certain parts of the molecule. The pulling down effect yields dents on the molecular surfaces. Some characteristic features are illustrated with arrows in Fig. 17. Since these anisotropic interactions originate from orbital interactions as shown in Fig. 12, drawbacks in the VDW models cannot be removed by semiempirical potentials such as Lennard-Jones (LJ) potentials based on isotropic pair potential functions, which have been widely used for molecular mechanics studies and also for analyses of scanning probe microscopic data.

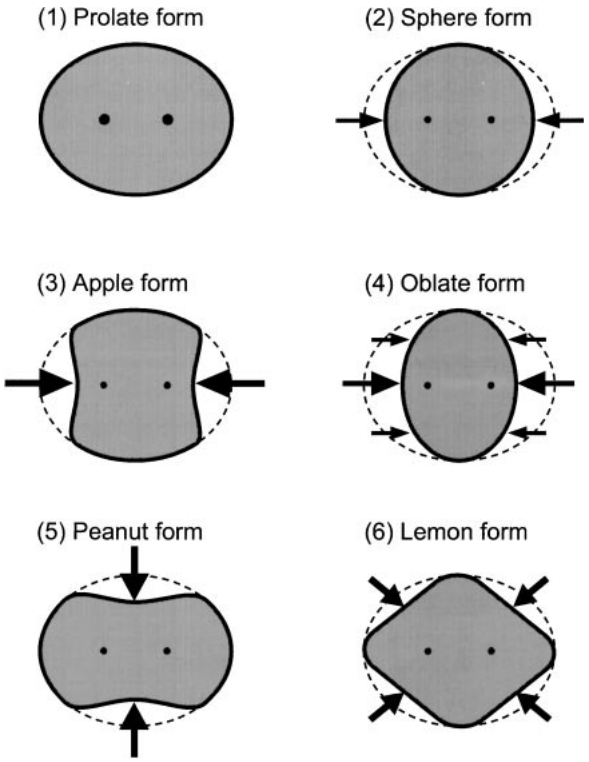

Fig. 17. Types of the outer shape of diatomic molecules probed by a test atom. Directions of anisotropic interactions pulling down repulsive potentials are specified by arrows.

External surfaces of molecules were thus found to be sensitive to anisotropic interactions. Shapes of N_2 and C_2H_2 in Fig. 15 demonstrate that the VDW models or the LJ models may be inappropriate even in qualitative levels of understanding. This should be of great significance in molecular recognition.

7. Experimental Determination of Molecular Orbitals

Although zero-point vibrations disturb molecular structures, we can determine geometrical molecular structures experimentally in terms of equilibrium bond lengths and bond angles based on the Born–Oppenheimer formalism and some additional approximate treatments. If there is a firm connection between experimental results and theoretical models, it may be possible to determine theoretical quantities by experiments. In quantum theoretical description of molecules, molecular orbitals are fundamental constructs, which are usually determined by self-consistent field molecular orbital (SCF-MO) methods. However, electron correlation effects are sometimes very important, especially for open-shell systems and excited electronic states. Nevertheless, experimental determination of molecular orbitals is a challenging target, since many experimental results obtained by electron spectroscopic techniques are more or less directly related with molecular orbitals for closed-shell systems in the ground electronic states.

As already mentioned in the forgoing sections, experimentally obtained CEDPICS can be related with the entrance interaction potential of V_* and the ionization width Γ. In our studies, observed CEDPICS could be reproduced from V_* and Γ via trajectory calculations. It is of note that V_* may also be determined from some scattering experiments. Thus, it is interesting to explore whether Γ can be constructed from CEDPICS and V_*. Since the ionization width Γ is related almost directly with target molecular orbitals, we tried to determine molecular orbital functions[155] based on the CEDPICS and V_* so far obtained. Molecular orbital coefficients and orbital exponents of atomic orbitals were optimized via trajectory calculations using V_* so that calculated CEDPICS may agree with observed CEDPICS. If we use wrong molecular orbitals clearly different from correct assignments to electron spectroscopic data, calculations were found to be very much different from experiments. When we used molecular orbitals with correct assignments in a crude level such as those of minimal bases, agreements between experiments and calculations became better but still far from satisfactory. Starting from crude orbitals functions of SCF-MO in minimal basis sets of STO-6G, we obtained optimized molecular orbitals (CEDPICS-MO) in terms of the minimal basis sets via trajectory calculations. Figure 18 demonstrates that electron distributions of the CEDPICS-MO in the minimal basis sets are in good agreement with those of the

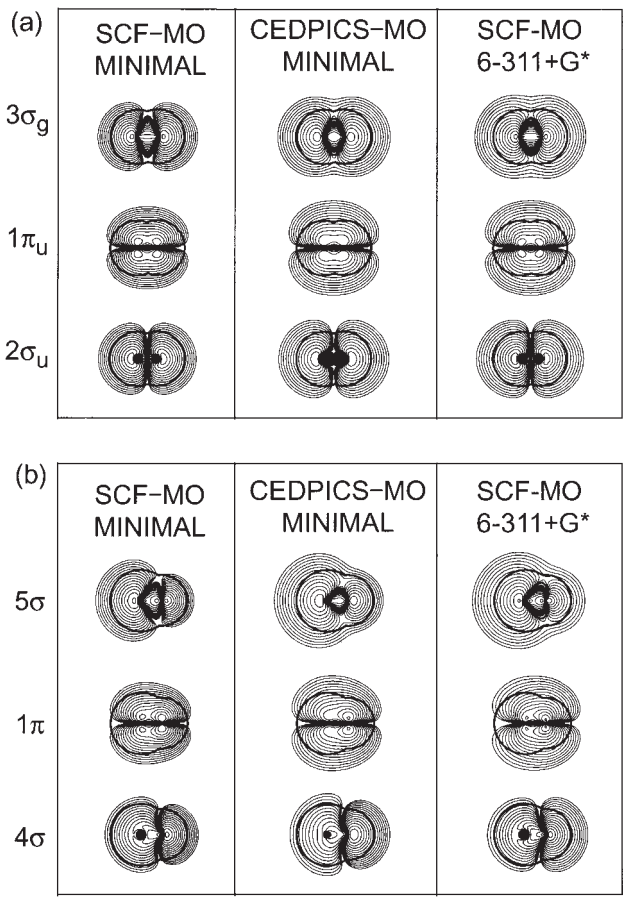

Fig. 18. Comparison of electron distributions of molecular orbitals of (a) N_2 and (b) CO. Crude SCF-MOs in a minimal basis of STO-6G are used for initial guess and denoted as SCF-MO/MINIMAL. Optimized molecular orbitals in the frame of a minimal set based on CEDPICS and V_* are denoted as CEDPICS-MO/MINIMAL. SCF-MOs with a 6-311+G* set are denoted as SCF-MO/6-311+G*.

higher level SCF-MO obtained with 6-311+G* basis sets. This indicates that experimental determination of molecular orbital coefficients together with optimization of atomic orbital exponents is possible. In other words, molecular orbital functions may be determined not by energy variational procedures but by observed 2D-PIES data including CEDPICS via trajectory calculations. When recently developed experimental techniques controlling molecular orientation and alignment[156,157] can be combined with 2D-PIES experiments, much more precise determination of molecular orbitals will become possible.

8. Concluding Remarks

The long quest for molecular orbitals and molecular surfaces has experienced many facets of scientific studies. Many obstacles had to be overcome in both experiments and theories. Some problems that initially seemed too difficult have been solved by step-by-step challenges developing new methods and techniques which had not been tested though they may be possible in principle. The present article summarizes brief histories of the author's quest for disclosing exterior characteristics of molecules by using atomic probes. Some related topics could not be described because of the limited space. Many other important aspects can also be traced via references. As mentioned in the last section, the quest may be continued further, since new experimental methods and theoretical techniques are in progress. In experiments, angular distributions of Penning electrons[158] and crossed molecular beam studies[159] will give valuable information on collisional ionization dynamics. In theories, some orbital descriptions including electron correlation effects, such as Dyson orbitals,[15] as well as more sophisticated potential energy surface calculations may provide further elucidation of molecular orbitals and molecular surfaces.

The author wishes to thank all people who gave important contributions to the topics in this article. Although the names of more than sixty peoples cannot be listed here, most of their names can be found together with the author's name in References cited below. The author also appreciates the technical contributions by staff members of machine shop and glass work shop at The University of Tokyo and Tohoku University. The author has been financially supported by the Ministry of Education, Culture, Sports, Science and Technology, by its Grants-in-Aid of Scientific Research No. 58470011, No. 61470014, No. 03403004, No. 07554024, and No. 14340173.

References

1 K. Fukui, *Int. J. Quantum Chem.*, **12**, 277 (1977).
2 K. Fukui, T. Yonezawa, and H. Shingu, *J. Chem. Phys.*, **20**, 722 (1952).
3 R. B. Woodward and R. Hoffmann, *Angew. Chem., Int. Ed. Engl.*, **8**, 781 (1969).
4 K. Siegbahn, C. Nordling, A. Fahlman, R. Nordberg, K. Hamrin, J. Hedman, G. Johansson, T. Bergmark, S.-E. Karlsson, I. Lindgren, and B. Lindberg, "ESCA-Atomic, Molecular and Solid State Structure Studied by Means of Electron Spectroscopy," Ser. IV, North-Holand Publishing Co., Amsterdam-London (1967), Vol. 20.
5 D. W. Turner, C. Baker, A. D. Baker, and C. R. Brundle, "Molecular Photoelectron Spectroscopy," Wiley, New York (1970).
6 K. Kimura, S. Katsumata, Y. Achiba, T. Yamazaki, and S. Iwata, "Handbook of He I Photoelectron Spectra of Fundamental Organic Molecules," Japan Scientific Societies Press, Tokyo (1981).
7 T. Koopmans, *Physica (Amsterdam)*, **1**, 104 (1933).
8 E. Weigold, S. T. Hood, and P. J. O. Teubner, *Phys. Rev. Lett.*, **30**, 475 (1972).
9 S. T. Hood, A. Hamnett, and C. E. Brion, *Chem. Phys. Lett.*, **39**, 252 (1976).
10 M. A. Coplan, J. H. Moore, and J. A. Tossel, *J. Chem. Phys.*, **68**, 329 (1978).
11 I. E. McCarthy and E. Weigold, *Endeavour*, **2**, 72 (1978).
12 A. O. Bagawan, R. Muller-Fiedler, C. E. Brion, E. R. Davidson, and C. Boyle, *Chem. Phys.*, **120**, 335 (1988).
13 M. A. Coplan, J. H. Moore, and J. P. Doering, *Rev. Mod. Phys.*, **66**, 985 (1994).
14 R. J. Nicholson, I. E. McCarthy, and W. Weyrich, *J. Phys. B: At. Mol. Opt. Phys.*, **32**, 3873 (1999).
15 E. Weigold and I. E. McCarthy, "Electron Momentum Spectroscopy," Kluwer Academic/Plenum, New York (1999).
16 P. G. Mezey, "Shape in Chemistry: An Introduction to Molecular Shape and Topology," VCH Publishers, New York (1993).
17 N. L. Max, *J. Mol. Graph.*, **2**, 8 (1984).
18 F. M. Richards, *Ann. Rev. Biophys. Bioeng.*, **6**, 151 (1977).
19 J. E. Dubois, J. P. Doucet, and S. Y. Yue, "Molecules in Physics, Chemistry, and Biology," ed by J. Maruani, Kluwer Academic, Dordrecht (1988), pp. 173–204.
20 R. H. Rohrbaugh and P. C. Jurs, *Anal. Chem.*, **59**, 1048 (1987).
21 T. Munakata, K. Ohno, and Y. Harada, *J. Chem. Phys.*, **72**, 2880 (1980).
22 F. M. Penning, *Naturwissenchaften*, **15**, 818 (1927).
23 A. J. Yencha, "Electron Spectroscopy: Theory, Techniques and Applications," ed by C. R. Brundle and A. D. Baker, Academic Press, New York (1984), Vol. 5.
24 P. E. Siska, *Rev. Mod. Phys.*, **65**, 337 (1993).
25 V. Čermák, *J. Chem. Phys.*, **44**, 3781 (1966).
26 A. Niehaus, *Adv. Chem. Phys.*, **45**, 399 (1981).
27 J. H. D. Eland, "Photoelectron Spectroscopy," Butterworths, London (1974).
28 H. Hotop and A. Niehaus, *Z. Phys.*, **228**, 68 (1969).
29 K. Ohno, H. Mutoh, and Y. Harada, *J. Am. Chem. Soc.*, **105**, 4555 (1983).
30 H. Hotop and A. Niehaus, *Int. J. Mass Spectrom. Ion Phys.*, **5**, 425 (1970).
31 D. S. C. Yee, W. B. Stewart, C. A. McDowell, and C. E. Brion, *J. Electron Spectrosc. Relat. Phenom.*, **7**, 377 (1975).
32 V. Čermák and A. J. Yencha, *J. Electron Spectrosc. Relat. Phenom.*, **8**, 109 (1976).
33 T. Munakata, K. Kuchitsu, and Y. Harada, *Chem. Phys. Lett.*, **64**, 409 (1979).
34 H. Hotop, E. Kolb, and J. Lorenzen, *J. Electron Spectrosc. Relat. Phenom.*, **16**, 213 (1979).
35 K. Ohno, S. Takano, and K. Mase, *J. Phys. Chem.*, **90**, 2015 (1986).
36 K. Ohno, S. Matsumoto, and Y. Harada, *J. Chem. Phys.*, **81**, 4447 (1984).
37 T. Munakata, K. Ohno, Y. Harada, and K. Kuchitsu, *Chem. Phys. Lett.*, **83**, 243 (1981).
38 T. Kajiwara, S. Masuda, K. Ohno, and Y. Harada, *J. Chem.*

Soc., Perkin Trans. 2, **1988**, 507.
39 K. Ohno, K. Imai, S. Matsumoto, and Y. Harada, *J. Phys. Chem.*, **87**, 4346 (1983).
40 S. Fujisawa, K. Ohno, S. Masuda, and Y. Harada, *J. Am. Chem. Soc.*, **108**, 6505 (1986).
41 K. Ohno, K. Imai, and Y. Harada, *J. Am. Chem. Soc.*, **107**, 8078 (1985).
42 K. Ohno, S. Matsumoto, K. Imai, and Y. Harada, *J. Phys. Chem.*, **88**, 206 (1984).
43 T. Munakata, Y. Harada, K. Ohno, and K. Kuchitsu, *Chem. Phys. Lett.*, **84**, 6 (1981).
44 Y. Harada, K. Ohno, and H. Mutoh, *J. Chem. Phys.*, **79**, 3251 (1983).
45 R. Hoffmann, *Angew. Chem., Int. Ed. Engl.*, **21**, 711 (1982).
46 D. M. P. Mingos, *Adv. Organomet. Chem.*, **15**, 1 (1977).
47 K. Ohno and Y. Harada, "Theoretical Models of Chemical Bonding," ed by Z. B. Maksić, Springer, Berlin (1991), Part 3, pp. 199–233.
48 K. Ohno, T. Ishida, Y. Naitoh, and Y. Izumi, *J. Am. Chem. Soc.*, **107**, 8082 (1985).
49 K. Ohno, S. Fujisawa, H. Mutoh, and Y. Harada, *J. Phys. Chem.*, **86**, 440 (1982).
50 M. Aoyama, S. Masuda, K. Ohno, Y. Harada, M. C. Yew, H. H. Hua, and L. S. Yong, *J. Phys. Chem.*, **93**, 1800 (1989).
51 R. Hoffmann, A. Imamura, and W. J. Hehre, *J. Am. Chem. Soc.*, **90**, 1499 (1968).
52 M. Yamauchi, Y. Yamakita, H. Yamakado, and K. Ohno, *J. Electron Spectrosc. Relat. Phenom.*, **88–91**, 155 (1998).
53 Y. Yamakita, M. Yamauchi, and K. Ohno, *Chem. Phys. Lett.*, **322**, 189 (2000).
54 M. Aoyama, S. Masuda, K. Ohno, Y. Harada, M. C. Yew, H. H. Hua, and L. S. Yong, *J. Phys. Chem.*, **93**, 5414 (1989).
55 T. Takami, K. Mitsuke, and K. Ohno, *J. Chem. Phys.*, **95**, 918 (1991).
56 W. Nakanishi, S. Masuda, T. Ishida, K. Ohno, and Y. Harada, *J. Org. Chem.*, **54**, 540 (1989).
57 N. Kishimoto, R. Yokoi, H. Yamakado, and K. Ohno, *J. Phys. Chem.*, **101**, 3284 (1997).
58 S. X. Tian, N. Kishimoto, and K. Ohno, *J. Electron. Spectrosc. Relat. Phenom.*, **127**, 167 (2002).
59 K. Ohno, S. Matsumoto, and Y. Harada, *J. Chem. Phys.*, **81**, 2183 (1984).
60 K. Ohno and T. Ishida, *Int. J. Quantum Chem.*, **29**, 677 (1986).
61 K. Ohno, *Theoret. Chim. Acta*, **74**, 239 (1988).
62 T. Ishida and K. Ohno, *Int. J. Quantum Chem.*, **32**, 257 (1989).
63 N. C. Handy, M. T. Marron, and H. J. Silverstone, *Phys. Rev.*, **180**, 180 (1969).
64 M. M. Morrell, R. G. Parr, and M. Levy, *J. Chem. Phys.*, **62**, 549 (1975).
65 T. Ishida and K. Ohno, *Theoret. Chim. Acta*, **81**, 355 (1992).
66 S. Tomoda, *Chem. Rev.*, **99**, 1243 (1999).
67 Y. Harada, S. Masuda, and H. Ozaki, *Chem. Rev.*, **97**, 1897 (1997).
68 J. P. Riola, J. S. Howard, R. D. Rundel, and R. F. Stebbings, *J. Phys. B*, **7**, 376 (1974).
69 W. Lindenger, A. L. Schmeltekopf, and F. C. Fehsenfelt, *J. Chem. Phys.*, **61**, 2890 (1974).
70 E. Illenberger and A. Niehaus, *Z. Phys. B*, **20**, 33 (1975).
71 A. Pesnelle, G. Watel, and C. Manus, *J. Chem. Phys.*, **62**, 3590 (1975).
72 M. R. Woodard, R. C. Sharp, M. Seely, and E. E. Muschlitz, Jr., *J. Chem. Phys.*, **69**, 2978 (1978).
73 L. Appoloni, B. Brunetti, J. Hermanussen, F. Vecchiocattivi, and G. G. Volpi, *J. Chem. Phys.*, **69**, 2978 (1978).
74 W. Allison and E. Muschlitz, Jr., *J. Electron Spectrosc. Relat. Phenom.*, **23**, 339 (1981).
75 T. P. Parr, D. M. Parr, and R. M. Martin, *J. Chem. Phys.*, **76**, 316 (1982).
76 K. Mitsuke, T. Takami, and K. Ohno, *J. Chem. Phys.*, **91**, 1618 (1989).
77 K. Ohno, T. Takami, K. Mitsuke, and T. Ishida, *J. Chem. Phys.*, **94**, 2675 (1991).
78 T. Takami and K. Ohno, *J. Chem. Phys.*, **96**, 6523 (1992).
79 K. Ohno, H. Yamakado, T. Ogawa, and T. Yamata, *J. Chem. Phys.*, **105**, 7536 (1996).
80 N. Kishimoto, J. Aizawa, H. Yamakado, and K. Ohno, *J. Phys. Chem.*, **101**, 5038 (1997).
81 N. Kishimoto, M. Furuhashi, and K. Ohno, *J. Electron Spectrosc. Relat. Phenom.*, **88–91**, 143 (1998).
82 K. Ohno, H. Tanaka, Y. Yamakita, R. Maruyama, T. Horio, and F. Misaizu, *J. Electron Spectrosc. Relat. Phenom.*, **112**, 115 (2000).
83 Y. Yamakita, H. Tanaka, R. Maruyama, H. Yamakado, F. Misaizu, and K. Ohno, *Rev. Sci. Instrum.*, **71**, 3042 (2000).
84 D. W. Fahey, W. F. Parks, and L. D. Schearer, *J. Phys. E*, **13**, 381 (1980).
85 H. G. Hecht, "Mathematics in Chemistry. An Introduction to Modern Methods," Prentice Hall, London (1990).
86 D. J. Auerbach, "Atomic and Molecular Beam Methods," ed by G. Scoles, Oxford University Press, New York-Oxford (1988), Vol. 1, pp. 362–379.
87 T. Pasinszki, H. Yamakado, and K. Ohno, *J. Phys. Chem.*, **97**, 12718 (1993).
88 K. Ohno, N. Kishimoto, and H. Yamakado, *J. Phys. Chem.*, **99**, 9687 (1995).
89 K. Ohno, K. Okamura, H. Yamakado, S. Hoshino, T. Takami, and M. Yamauchi, *J. Phys. Chem.*, **99**, 14247 (1995).
90 T. Pasinszki, H. Yamakado, and K. Ohno, *J. Phys. Chem.*, **99**, 14678 (1995).
91 H. Yamakado, M. Yamauchi, S. Hoshino, and K. Ohno, *J. Phys. Chem.*, **99**, 17093 (1995).
92 N. Kishimoto, H. Yamakado, and K. Ohno, *J. Phys. Chem.*, **100**, 8204 (1996).
93 H. Yamakado, K. Okamura, K. Ohshimo, N. Kishimoto, and K. Ohno, *Chem. Lett.*, **1997**, 269.
94 H. Yamakado, T. Ogawa, and K. Ohno, *J. Phys. Chem.*, **101**, 3887 (1997).
95 M. Yamauchi, H. Yamakado, and K. Ohno, *J. Phys. Chem.*, **101**, 6184 (1997).
96 H. Tanaka, H. Yamakado, and K. Ohno, *J. Electron Spectrosc. Relat. Phenom.*, **88–91**, 149 (1998).
97 N. Kishimoto, K. Ohshimo, and K. Ohno, *J. Elecrtron Spectrosc. Relat. Phenom.*, **104**, 145 (1999).
98 T. Pasinszki, N. Kishimoto, and K. Ohno, *J. Phys. Chem. A*, **103**, 6746 (1999).
99 T. Pasinszki, N. Kishimoto, T. Ogawa, and K. Ohno, *J. Phys. Chem. A*, **103**, 7170 (1999).
100 T. Pasinszki, N. Kishimoto, and K. Ohno, *J. Phys. Chem. A*, **103**, 9195 (1999).
101 N. Kishimoto, Y. Osada, and K. Ohno, *J. Phys. Chem. A*, **104**, 1393 (2000).
102 N. Kishimoto and K. Ohno, *J. Phy. Chem. A*, **104**, 6940

(2000).
103 N. Kishimoto, M. Furuhashi, and K. Ohno, *J. Electron Spectrosc. Relat. Phenom.*, **113**, 35 (2000).
104 M. Yamazaki, N. Kishimoto, M. Kurita, T. Ogawa, K. Ohno, and K. Takeshita, *J. Electron Spectrosc. Relat. Phenom.*, **114–116**, 175 (2001).
105 N. Kishimoto, Y. Osada, and K. Ohno, *J. Electron Spectrosc. Relat. Phenom.*, **114–116**, 183 (2001).
106 K. Imura, N. Kishimoto, and K. Ohno, *J. Phys. Chem. A*, **105**, 4189 (2001).
107 K. Imura, N. Kishimoto, and K. Ohno, *J. Phys. Chem. A*, **105**, 6073 (2001).
108 K. Imura, N. Kishimoto, and K. Ohno, *J. Phys. Chem. A*, **105**, 6378 (2001).
109 K. Imura, N. Kishimoto, and K. Ohno, *J. Phys. Chem. A*, **105**, 9111 (2001).
110 K. Imura, N. Kishimoto, and K. Ohno, *J. Phys. Chem. A*, **105**, 10787 (2001).
111 K. Kanda, Y. Yamakita, and K. Ohno, *Chem. Phys. Lett.*, **349**, 411 (2001).
112 K. Imura, N. Kishimoto, and K. Ohno, *J. Phys. Chem. A*, **106**, 3759 (2002).
113 N. Kishimoto, H. Ogasawara, and K. Ohno, *Bull. Chem. Soc. Jpn.*, **75**, 1503 (2002).
114 S. X. Tian, N. Kishimoto, and K. Ohno, *J. Phys. Chem. A*, **106**, 6541 (2002).
115 S. X. Tian, N. Kishimoto, and K. Ohno, *J. Electron Spectrosc. Relat. Phenom.*, **125**, 205 (2002).
116 S. X. Tian, N. Kishimoto, and K. Ohno, *J. Phys. Chem. A*, **106**, 7714 (2002).
117 S. X. Tian, N. Kishimoto, and K. Ohno, *Chem. Phys. Lett.*, **365**, 40 (2002).
118 S. X. Tian, N. Kishimoto, and K. Ohno, *J. Phys. Chem. A*, **107**, 53 (2003).
119 S. X. Tian, N. Kishimoto, and K. Ohno, *J. Phys. Chem. A*, **107**, 485 (2003).
120 S. X. Tian, N. Kishimoto, and K. Ohno, *J. Phys. Chem. A*, **107**, 2137 (2003).
121 T. Hsu and J. L. Hirshfield, *Rev. Sci. Instrum.*, **4**, 236 (1976).
122 G. Beamson, H. Q. Porter, and D. W. Turner, *J. Phys. E*, **13**, 64 (1980).
123 G. Beamson, H. Q. Porter, and D. W. Turner, *Nature*, **290**, 556 (1981).
124 P. Kruit and F. H. Read, *J. Phys. E*, **16**, 313 (1983).
125 H. Tanaka, R. Maruyama, Y. Yamakita, H. Yamakado, F. Misaizu, and K. Ohno, *J. Chem. Phys.*, **112**, 7062 (2000).
126 R. Maruyama, H. Tanaka, Y. Yamakita, F. Misaizu, and K. Ohno, *Chem. Phys. Lett.*, **327**, 104 (2000).
127 H. Yamakado, H. Tanaka, R. Maruyama, Y. Yamakita, F. Misaizu, and K. Ohno, "International Conference on Photonic, Electronic, and Atomic Collisions," 22th ICPEAC, Santa Fe (2001), p. 678.
128 T. Ogawa and K. Ohno, *J. Chem. Phys.*, **110**, 3773 (1999).
129 T. Ogawa and K. Ohno, *J. Phys. Chem. A*, **103**, 9925 (1999).
130 K. Ohno, M. Yamazaki, N. Kishimoto, T. Ogawa, and K. Takeshita, *Chem. Phys. Lett.*, **332**, 167 (2000).
131 M. Yamazaki, S. Maeda, N. Kishimoto, and K. Ohno, *Chem. Phys. Lett.*, **355**, 311 (2002).
132 M. Yamazaki, S. Maeda, N. Kishimoto, and K. Ohno, *J. Chem. Phys.*, **117**, 5707 (2002).
133 N. Kishimoto, T. Horio, S. Maeda, and K. Ohno, *Chem. Phys. Lett.*, **379**, 332 (2003).
134 S. Maeda, M. Yamazaki, N. Kishimoto, and K. Ohno, *J. Chem. Phys.*, **120**, 781 (2004).
135 M. Yamazaki, S. Maeda, and K. Ohno, submitted for publication.
136 H. Hotop, *Radiat. Res.*, **59**, 379 (1974).
137 H. Haberland, Y. T. Lee, and P. E. Siska, *Adv. Chem. Phys.*, **45**, 487 (1981).
138 H. Hotop, T. E. Roth, M.-W. Ruf, and A. J. Yencha, *Theor. Chem. Acc.*, **100**, 36 (1998).
139 L. S. Cederbaum, *J. Phys. B*, **8**, 290 (1975).
140 J. V. Ortiz, *J. Chem. Phys.*, **104**, 7599 (1996).
141 V. F. Lotrich and A. van der Avoird, *J. Chem. Phys.*, **118**, 1110 (2003).
142 R. E. Olson, F. T. Smith, and E. Bauer, *Appl. Opt.*, **10**, 1848 (1971).
143 R. E. Olson, *Phys. Rev.*, **6**, 1031 (1972).
144 E. J. Longley, D. C. Dunlavy, M. F. Falcetta, H. M. Bevsek, and P. E. Siska, *J. Phys. Chem.*, **97**, 2097 (1993).
145 D. C. Dunlavy and P. E. Siska, *J. Phys. Chem.*, **100**, 21 (1996).
146 T. Ishida and H. Katagiri, *J. Phys. Chem.*, **105**, 9379 (2001).
147 T. Ishida, *Chem. Phys. Lett.*, **191**, 1 (1992).
148 W. H. Miller and H. Morgner, *J. Chem. Phys.*, **67**, 4923 (1977).
149 R. S. Mulliken, *J. Chim. Phys.*, **46**, 497 (1949).
150 V. N. Demikov, *Soviet Phys. JETP*, **18**, 138 (1964).
151 S.-I. Choi, J. Jortner, S. A. Rice, and R. Silbey, *J. Chem. Phys.*, **41**, 3294 (1964).
152 W. H. Press, S. A. Teukolsky, W. T. Vetterling, and B. P. Flannery, "Numerical Recipes in C," Cambridge University Press, Cambridge (1988).
153 S. Hoshino and K. Ohno, *Elec. J. Theoret. Chem.*, **2**, 1 (1997).
154 S. Hoshino and K. Ohno, *J. Am. Chem. Soc.*, **119**, 8276 (1997).
155 M. Yamazaki, S. Maeda, and K. Ohno, submitted for publication.
156 F. Pirani, M. Bartolomei, V. Aquilanti, M. Scotoni, M. Vescovi, D. Ascenzi, D. Bassi, and D. Cappelletti, *J. Chem. Phys.*, **119**, 265 (2003).
157 K. Koizumi, H. Ohoyama, S. Okada, and T. Kasai, *J. Chem. Phys.*, **118**, 5395 (2003).
158 K. Mitsuke, K. Kusafuka, and K. Ohno, *J. Phys. Chem.*, **93**, 3062 (1989).
159 T. Horio, R. Maruyama, N. Kishimoto, and K. Ohno, *Chem. Phys. Lett.*, **384**, 73 (2004).

Koichi Ohno Professor at Department of Chemistry, Graduate School of Science, Tohoku University, was born on September 19, 1945. He graduated from The University of Tokyo in 1968 and obtained the degree of Doctor of Science in 1973 under the supervison of Professor Hiroo Inokuchi. He worked at the College of Arts and Sciences, The University of Tokyo, as Research Associate for 1972–1980, as Associate Professor for 1980–1989, as Professor for 1989–1994. Then, he moved to the Department of Chemistry, Faculty of Science, Tohoku University in 1994. Since then he has been Professor at Tohoku University. During 1975–1977 he was a Ramsay Fellow at the Department of Chemistry, The University of Sheffield, UK. His scientific interests are related with many fields of molecular science, both in experiment and theory, in particular molecular spectroscopy, electron spectroscopy, and quantum chemistry.